Entropy Scaling Framework for Transport Properties using Molecular-based Equations of State

Sebastian Schmitt, Hans Hasse, and Simon Stephan[a)]

Laboratory of Engineering Thermodynamics (LTD), RPTU Kaiserslautern, Kaiserslautern 67663, Germany

(Dated: 2024-01-09)

Modeling transport properties is important for many applications. In this work, an entropy scaling framework for modeling transport properties using molecular-based equations of state (EOS) is presented. It can be applied for modeling the viscosity, thermal conductivity, and self-diffusion coefficients. The framework is formulated in a general way such that it can be coupled with various EOS. It is demonstrated that the model, when coupled to molecular-based EOS, provides not only good descriptions of existing data but also reasonable predictions in a wide range of states covering liquid, gaseous, supercritical, and metastable regions. Moreover, the model can be used for reliably predicting transport properties of mixtures. The universal parameters of the model were fitted to computer experiment data of the Lennard-Jones fluid. This procedure provides inherently a robust form of the basic scaling function. Thereby, only few data points are required for the determination of the component-specific model parameters. The applicability of the developed framework is demonstrated for model fluids as well as for a wide variety of real substances including non-polar, polar, and associating pure fluids and mixtures.

[a)]Electronic mail: simon.stephan@rptu.de

I. INTRODUCTION

Transport properties of pure fluids and fluid mixtures are important in many disciplines of science and engineering[1,2]. In many cases, also transport properties at conditions, that are far away from the region in which data are available, have to be known. For example, in tribological applications[3,4], information on the viscosity at pressures above 1 GPa is required[5]. Other examples stem from carbon capture and storage[6], petroleum industry[7,8], power engineering[9,10], process engineering[1,11–13], and combustion processes[14]. Experimental transport property data are often only available for moderate conditions and for pure fluids; transport property data for extreme conditions and mixtures are scarce. Moreover, for a large number of relevant substances, even at moderate conditions, only little or no data are available. For modeling dynamic processes at interfaces[13,15,16], information on transport properties is also required in the metastable and unstable region[12,17,18], where practically no experimental data are available. Hence, reliable and predictive models for transport properties are required – which is challenging as transport properties vary strongly depending on the chosen conditions. Fig. 1 illustrates the viscosity, the thermal conductivity, and the self-diffusion coefficient for a molecular fluid in a phase diagram[19]; a detailed discussion of these topologies is given in the Supplementary Material.

Entropy scaling is an interesting method for the modeling of the viscosity, thermal conductivity, and self-diffusion coefficient. It is based on the discovery that the three properties are (within certain limits) monovariate functions of the configurational entropy – when properly scaled by the density and the temperature. The entropy scaling approach was originally proposed by *Rosenfeld* in 1977[20] and 1999[21]. Entropy scaling can be favorably coupled with equations of state (EOS)[22] that are used for modeling the configurational entropy as a function of, for example, temperature and pressure $s_{\mathrm{conf}} = s_{\mathrm{conf}}(T, p)$. Therefore, an accurate description of the configurational entropy is crucial for entropy scaling. For predicting the transport properties in state regions where no experimental data are available, a reliable extrapolation behavior of the entropy scaling model itself is required as well as reliable predictions for the configurational entropy $s_{\mathrm{conf}} = s_{\mathrm{conf}}(T, p)$ in that region. Several entropy scaling approaches have been proposed in recent years using empirical multi-parameter EOS models[23–29]. Empirical EOS, however, often lack of a robust extrapolation behavior. Molecular-based EOS, on the other hand, enable reliable extrapolations

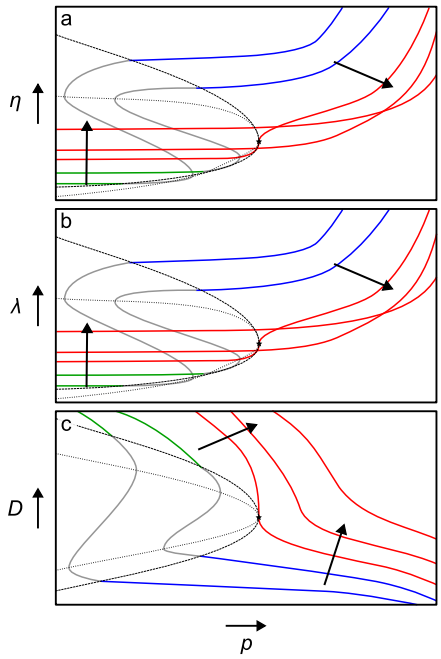

FIG. 1. Schematic diagrams with subcritical and supercritical isotherms for the viscosity (a), thermal conductivity (b), and self-diffusion coefficient (c) as a function of the pressure p. The isotherms are: two subcritical isotherms in the homogeneous liquid phase region (blue), in the homogeneous gas phase region (green), the metastable and the unstable region (grey), and the critical and supercritical (red) region. The binodal is indicated as solid line, the spinodal as dotted line, and the critical point by a star. The arrows indicate increasing temperature of the isotherms. The diagrams were drawn based on the entropy scaling models of a simple fluid.

including mixtures[30–36]. Some entropy scaling models that use molecular-based EOS have been proposed in the past: *Gross* and co-workers have developed entropy scaling models specifically for PC-SAFT[37–43]. The PC-SAFT EOS was also used by other authors to create entropy scaling models for the viscosity, the thermal conductivity, and the self-diffusion coefficient[44–50]. Yet, the PC-SAFT EOS has a physically unrealistic behavior at extreme conditions[51–54]. Also cubic EOS were used in entropy scaling models[47–49,55,56]. Entropy scaling was also applied to the transport properties of model fluids like the Lennard-Jones (LJ) fluid using specific LJ EOS[24,57–59]. As these models were specifically developed for a given EOS, they cannot be straightforwardly transferred to other EOS (that might provide a better description of the thermodynamic properties of the fluid). Hence, no generalized entropy scaling model has been developed yet that can be straightforwardly coupled with

different molecular-based EOS.

The core of the entropy scaling approach is the conversion of the transport properties to the so-called 'macroscopically scaled' quantities. *Rosenfeld*[20,21] found a monovariate relation of a macroscopically scaled transport property as a function of the configurational entropy s_{conf}. These findings were later elaborated in the isomorph theory[60,61]. The macroscopic *Rosenfeld*[20,21] scaling is only exact for some simple model potentials, e.g. for the inverse power-law potential[22]. For more complex model potentials (even the LJ potential) and real substances, there are deviations from this monovariate behavior[62] and the relation between the configurational entropy and the transport properties cannot be predicted a priori from the theory. Therefore, (component-specific) adjustable parameters are introduced for these substances.

In the present work, a generalized framework for the application of entropy scaling in conjunction with molecular-based EOS is proposed, which can be used for modeling transport properties of model fluids as well as real substances. The framework is designed such that the viscosity, the thermal conductivity, and the self-diffusion coefficient can be described. The new framework is based on a scaling of the three properties, that combines the *Rosenfeld* scaling with a scaling for the zero-density limit. The transition between the two approaches is achieved in a convenient, yet not physically rigorously deducible way. The universal parameters of the entropy scaling framework were fitted to computer experiment data for transport properties and the entropy of the LJ fluid, so that they do not depend on the chosen EOS. Therefore, simulations of the LJ fluid were conducted in which the transport properties and the entropy were sampled simultaneously. This makes the model on one hand robust and on the other hand flexible as it can be straightforwardly coupled with basically any EOS. For modeling a specific real substance, the entropy scaling model requires component-specific parameters, which have to be adjusted to experimental data of transport properties. The number of component-specific parameters of the model is 2-5 and can be chosen depending on the amount and quality of transport data that are available for the training. Hence, the model can also be applied in a meaningful way if only very few data are available. Based on the component-specific parameters for the pure substances, the framework can be applied to predict the viscosity and the thermal conductivity of mixtures without any additional information.

We demonstrate the flexibility of the entropy scaling framework by applying it to nine

different molecular-based EOS. Also, the robust extrapolation behavior of the framework to high pressures, metastable and unstable states, as well as mixtures is demonstrated. For mixtures, it is shown that transport properties can be predicted by the framework without the adjustment of additional parameters – even for highly non-ideal mixtures.

The paper is organized as follows: First, the entropy scaling framework is described, including the scaling procedure, the treatment of the zero-density limit, and the determination of the universal parameters. Then, the applicability of the framework is demonstrated for different pure substances and mixtures. Finally, conclusions are drawn.

II. MODEL

The principles of the entropy scaling framework developed in this work are depicted in Fig. 2. It can be applied for modeling the viscosity, the thermal conductivity, and the self-

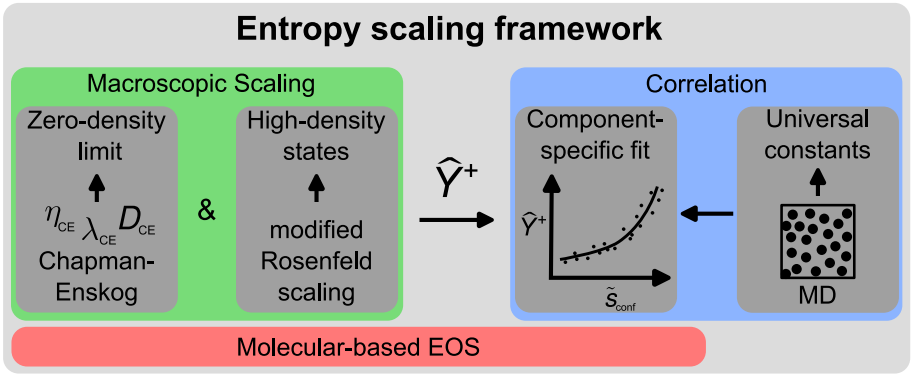

FIG. 2. Scheme of the entropy scaling framework proposed in this work.

diffusion coefficient of pure component fluids; and for modeling the viscosity and the thermal conductivity of fluid mixtures. The entropy scaling framework consists of two parts: a suitable macroscopic scaling of the transport properties (green part in Fig. 2) and correlations that describe the scaled data (blue part in Fig. 2). The scaling part comprises two different methods, one for the low-density region and one for the high-density region. The scaling is carried out so that the scaled properties from both regions fall onto a single continuous smooth curve describing the dependency of the scaled property on the configurational entropy. The mathematical function that is used here for describing this relation has both universal parameters that determine basic features of the function and component-specific parameters that have to be fitted to experimental data. The universal parameters were

fitted to molecular dynamics (MD) simulation results of the transport properties and the entropy of the LJ fluid determined in this work, i.e. without using an EOS. For applying the entropy scaling framework, it is coupled with a molecular-based EOS that yields the configurational entropy for the state point of interest, i.e. $s_{\mathrm{conf}}(T, \rho, \underline{x})$, where $\underline{x}$ indicates the composition vector of a mixture.

A. Molecular-based EOS

Molecular-based EOS are algebraic models for describing thermodynamic properties of fluids and fluid mixtures[30,31]. They are usually formulated in the *Helmholtz* energy per particle $a = A/N$ as a function of the temperature, density, and composition, i.e. $a = a(T, \rho, \underline{x})$, since this is a thermodynamic fundamental expression. All other thermodynamic properties can be derived from it[63]. In molecular-based EOS, the formulation of the *Helmholtz* energy is physically motivated and can be divided into an ideal gas and a configurational (or residual) contribution. The configurational contribution is usually constructed as a sum of terms in molecular-based EOS, each modeling the effect of a given molecular interaction or molecular architecture feature on the *Helmholtz* energy, for example, repulsion, attraction, association[64], electrostatic interactions[30], the chain formation[65] and branching in the molecular structure[66]. Hence, the configurational *Helmholtz* energy a_{conf} can be written as

$$a_{\mathrm{conf}} = a_{\mathrm{rep}} + a_{\mathrm{disp}} + a_{\mathrm{chain}} + a_{\mathrm{branching}} + a_{\mathrm{assoc}} + a_{\mathrm{D}} + a_{\mathrm{Q}}, \tag{1}$$

where a_{rep}, a_{disp}, a_{chain}, $a_{\mathrm{branching}}$, a_{assoc}, a_{D}, and a_{Q} indicate the contributions due to repulsive and dispersive interactions of monomers, the chain formation of multiple monomers, branching, associating (H-bonding) interactions, dipole interactions, and quadrupole interactions, respectively[67]. The terms contain different component-specific parameters, which can be physically interpreted. In different molecular-based EOS, different terms are combined to constitute the EOS. Component-specific parameters are for example the segment diameter σ, the segment dispersion energy ε, and the chain length, i.e. segment number or elongation parameter m. These component-specific parameters are usually fitted to experimental data – in particular to vapor-liquid equilibrium (VLE) properties and liquid phase densities.

Many different molecular-based EOS have been described in the literature[30], e.g. the BACKONE EOS family of *Fischer* and co-workers[68,69], the PACT EOS family of *Prausnitz*

and co-workers[70,71], the EOS family that uses the statistical association fluid theory (SAFT) of *Chapman*, *Jackson*, and *Gubbins*[64,72], and the CPA EOS family of *Kontogeorgis* and co-workers[73,74]. Since different molecular-based EOS are based on different modeling approaches and approximations, they differ in parts significantly in their mathematical formulation. Accordingly, for a given component, the component-specific parameters are not transferable among different molecular-based EOS.

Due to their sound physical basis, molecular-based EOS often enable reliable predictions for states and properties that were not considered in the training[30,31,52,67,75,76], i.e. many of them can be reliably applied not only for describing stable gas, liquid, and supercritical states, but also metastable and to some extend unstable states (which is for example relevant for interfaces). Yet, without further modifications[77], the critical point is not well described by most EOS. They overestimate the critical temperature and pressure (due to the underlying critical scaling behavior). For modeling mixtures with molecular-based EOS, mixing and combination rules are applied[30,32,33,78,79]. Thereby, it is usually sufficient to use a single state independent parameter ξ_{ij}, which is generally introduced in the *Berthelot* term, with which the binary dispersive cross-interactions ε_{ij} are described[80]

$$\varepsilon_{ij} = \xi_{ij}\sqrt{\varepsilon_i \varepsilon_j}, \tag{2}$$

where ε_i and ε_j are the dispersive interaction parameters of the pure components.

For entropy scaling, the calculation of the molar configurational entropy s_{conf} at a given state point $(T, \rho, \underline{x})$ is required. It can be calculated from the configurational *Helmholtz* energy a_{conf} as the derivative with respect to temperature T at constant volume v and composition $\underline{x}$

$$s_{\mathrm{conf}} = -\left(\frac{\partial a_{\mathrm{conf}}}{\partial T}\right)_{v,\underline{x}}. \tag{3}$$

In this work, nine molecular-based EOS were used: three LJ EOS (Kolafa-Nezbeda[81], PeTS[82], *Stephan* et al.[83]), three from the SAFT EOS family (PC-SAFT[65], SAFT-VR Mie[84], soft SAFT[85]), one from the PACT EOS family (PACT+B[70]), one from the BACKONE family[69], and one from the cubic EOS family (sCPA[73,86]). The pure component model parameters were taken from the literature[65,69,70,74,84,85,87–91]. Details are given in the Supplementary Material.

B. Scaling of the Transport Properties

The scaling of the viscosity η, the thermal conductivity λ, and the self-diffusion coefficient D with respect to temperature and density is the core of entropy scaling[20,21]. Here, a modified *Rosenfeld* scaling from *Bell*[24,62] (indicated by $^+$) is adopted:

$$\eta^+ = \eta \frac{\rho_\mathrm{N}^{-2/3}}{\sqrt{MTk_\mathrm{B}/N_\mathrm{A}}} \left(\frac{-s_\mathrm{conf}}{R}\right)^{2/3}, \tag{4}$$

$$\lambda^+ = \lambda \frac{\rho_\mathrm{N}^{-2/3}}{k_\mathrm{B}\sqrt{RT/M}} \left(\frac{-s_\mathrm{conf}}{R}\right)^{2/3}, \tag{5}$$

$$D^+ = D \frac{\rho_\mathrm{N}^{1/3}}{\sqrt{RT/M}} \left(\frac{-s_\mathrm{conf}}{R}\right)^{2/3}, \tag{6}$$

where ρ_N is the number density in $1/\mathrm{m}^3$, M the molar mass in kg/mol, $R = k_\mathrm{B}N_\mathrm{A}$ the universal gas constant, k_B the *Boltzmann* constant, and N_A the *Avogadro* number. The scaled transport properties Y^+ with $Y \in \{\eta, \lambda, D\}$ obtained from Eqs. (4) - (6) are dimensionless. This scaling approach yields an approximately monovariate dependency of Y^+ on the configurational entropy for dense states. However, this does not hold for low density states[21,92]. To overcome this drawback, a reduction using the *Chapman-Enskog* (CE) transport properties is applied here for low-densities as explained in more detail below.

Fig. 3 schematically shows the scaling procedure introduced in this work starting from Y^+ (green, cf. Eqs. (4) - (6)). In the framework, the reduced configurational entropy $\tilde{s}_\mathrm{conf}$ is defined as

$$\tilde{s}_\mathrm{conf} = \frac{-s_\mathrm{conf}}{m\,R}. \tag{7}$$

Therein, the segment number m describes the elongation of a molecule in a given molecular-based EOS and is used to scale s_conf such that the values of $\tilde{s}_\mathrm{conf}$ are within a similar range for molecules of different sizes[37]. Moreover, $\tilde{s}_\mathrm{conf}$ is also a dimensionless property. The limit $\tilde{s}_\mathrm{conf} \to 0$ corresponds to the limit $\rho \to 0$. Based on $\tilde{s}_\mathrm{conf}$, a split for individually describing the low-density (LD) and high-density (HD) region is applied. The LD region covers all states $\tilde{s}_\mathrm{conf} < \tilde{s}_\mathrm{conf}^\times$ and the HD region all states $\tilde{s}_\mathrm{conf} \geq \tilde{s}_\mathrm{conf}^\times$. Here, a value of $\tilde{s}_\mathrm{conf}^\times = 0.5$ was chosen based on preliminary studies.

The scaling with Eqs. (4) - (6) usually yields very good results for the HD region, but scattering results for the LD region (cf. Fig. 3, green part in the LD region). This scattering can be understood as a consequence of the known temperature-dependence of the results

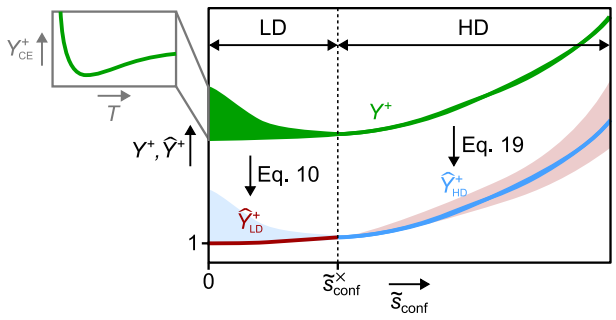

FIG. 3. Scheme illustrating the modeling principle of the entropy scaling framework. LD and HD indicate the low-density and the high-density region, respectively. Green indicates the scaled transport property Y^+ for a given substance with $Y \in \{\eta, \lambda, D\}$. Y^+_{CE} (left inset) indicates the zero-density limit transport property ($\rho \to 0$, $\tilde{s}_{\mathrm{conf}} \to 0$) obtained from *Chapman-Enskog* theory as function of the temperature T. $\widehat{Y}^+_{\mathrm{LD}}$ indicates the CE-scaled transport property in the LD region (cf. Eq. (14)) and $\widehat{Y}^+_{\mathrm{HD}}$ the CE-scaled transport property in the HD region (cf. Eq. (15)). The light red and light blue areas are not used.

for $\rho \to 0$, as described by the *Chapman-Enskog* theory, cf. insert in Fig. 3. Applying Eqs. (4) - (6) to the results from the *Chapman-Enskog* theory yields:

$$\eta^+_{\mathrm{CE}} = \frac{5}{16\sqrt{\pi}} \frac{1}{\sigma^2_{\mathrm{CE}} \Omega^{(2,2)}} \left(T \left(\frac{\mathrm{d}B}{\mathrm{d}T} \right) + B \right)^{2/3}, \tag{8}$$

$$\lambda^+_{\mathrm{CE}} = \frac{75}{64\sqrt{\pi}} \frac{1}{\sigma^2_{\mathrm{CE}} \Omega^{(2,2)}} \left(T \left(\frac{\mathrm{d}B}{\mathrm{d}T} \right) + B \right)^{2/3}, \tag{9}$$

$$D^+_{\mathrm{CE}} = \frac{3}{8\sqrt{\pi}} \frac{1}{\sigma^2_{\mathrm{CE}} \Omega^{(1,1)}} \left(T \left(\frac{\mathrm{d}B}{\mathrm{d}T} \right) + B \right)^{2/3}, \tag{10}$$

where the relation

$$\lim_{\rho_{\mathrm{N}} \to 0} \left(\frac{\partial(-s_{\mathrm{conf}}/R)}{\partial \rho_{\mathrm{N}}} \right)_T = T \frac{\mathrm{d}B}{\mathrm{d}T} + B \tag{11}$$

is exploited with B being the second virial coefficient (computed from the EOS) and $\Omega^{(1,1)}$ and $\Omega^{(2,2)}$ are the reduced collision integrals[93], which are functions of the reduced temperature $Tk_{\mathrm{B}}/\varepsilon_{\mathrm{CE}}$, i.e. $\Omega^{(1,1)} = \Omega^{(1,1)}(Tk_{\mathrm{B}}/\varepsilon_{\mathrm{CE}})$ and $\Omega^{(2,2)} = \Omega^{(2,2)}(Tk_{\mathrm{B}}/\varepsilon_{\mathrm{CE}})$. The two parameters σ_{CE} and $\varepsilon_{\mathrm{CE}}$ characterize the molecular size and dispersion energy, respectively. The scaled *Chapman-Enskog* transport properties η^+_{CE}, λ^+_{CE}, and D^+_{CE} are solely functions of the temperature. In the Supplementary Material, the Eqs. (8) - (9) are derived from the *Chapman-Enskog* equations. The LJ fluid is taken as a reference fluid for calculating the zero-density limit transport properties; the empirical correlations for the collision integrals

for the LJ fluid from *Kim* and *Monroe* were used[94]. To determine the parameters σ_{CE} and $\varepsilon_{\mathrm{CE}}$, the LJ model is mapped to a given real substance by applying the corresponding states principle. Hence, σ_{CE} and $\varepsilon_{\mathrm{CE}}$ are determined from the critical temperature T_{c} and pressure p_{c} of the considered substance and the critical temperature and pressure of the LJ fluid as

$$\varepsilon_{\mathrm{CE}} = \frac{T_{\mathrm{c}}}{T_{\mathrm{c,LJ}}/\varepsilon_{\mathrm{LJ}}}, \tag{12}$$

$$\sigma_{\mathrm{CE}} = \left(\frac{\left(p_{\mathrm{c,LJ}} \sigma_{\mathrm{LJ}}^3 / \varepsilon_{\mathrm{LJ}} \right) \varepsilon_{\mathrm{CE}}}{p_{\mathrm{c}}} \right)^{1/3}, \tag{13}$$

where $\varepsilon_{\mathrm{LJ}}$ and σ_{LJ} indicate the size and energy parameter of the LJ potential, respectively. The reduced critical temperature and pressure of the LJ fluid were taken from the literature: $T_{\mathrm{c,LJ}} = 1.321\ \varepsilon_{\mathrm{LJ}}/k_{\mathrm{B}}$ and $p_{\mathrm{c,LJ}} = 0.316\ \varepsilon_{\mathrm{LJ}}/\sigma_{\mathrm{LJ}}^3$ [95]. Thus, Eqs. (12) - (13) establish a link between the real substance model described by the molecular-based EOS and the LJ model in the zero-density limit. The critical parameters T_{c} and p_{c} for a given substance are taken from the EOS.

The CE-scaled transport property for the LD region $\widehat{Y}_{\mathrm{LD}}^+$ (with $Y \in \{\eta, \lambda, D\}$) is calculated from Y_{LD}^+ as

$$\widehat{Y}_{\mathrm{LD}}^+ = \frac{Y_{\mathrm{LD}}^+}{Y_{\mathrm{CE}}^+}. \tag{14}$$

As illustrated in Fig. 3, $\widehat{Y}_{\mathrm{LD}}^+$ provides a monovariate function with respect to the reduced configurational entropy $\tilde{s}_{\mathrm{conf}}$. In the case of exact representation of the zero-density limit of the transport properties by the *Chapman-Enskog* theory, Eq. (14) yields unity ($\widehat{Y}^+ = 1$) for $\tilde{s}_{\mathrm{conf}} \to 0$. Applying Eq. (14) to all states including the HD region would, however, yield a distinctly poorer scaling than in the LD region, as illustrated in Fig. 3. As the modified *Rosenfeld* scaling already yields a decent behavior in the HD region, the scaled transport property for the HD region Y_{HD}^+ only has to be shifted in a suitable way to obtain a smooth transition in $\widehat{Y}^+$ from the LD to the HD region at $\tilde{s}_{\mathrm{conf}}^{\times}$. Preliminary studies showed that this can be achieved by simply dividing Y^+ by a constant factor for which the minimum of the scaled *Chapman-Enskog* transport property $\min(Y_{\mathrm{CE}}^+(T))$ was chosen, i.e.

$$\widehat{Y}_{\mathrm{HD}}^+ = \frac{Y_{\mathrm{HD}}^+}{\min\left(Y_{\mathrm{CE}}^+(T)\right)}. \tag{15}$$

The rationale behind this choice is that the scattering of Y^+ can be understood as positive deviations from a master curve that extends the results from the HD region (cf. green part

in Fig. 3). By dividing the results from the HD region by the minimum value from the *Chapman-Enskog* theory, it can be expected to recover this curve, albeit in a version that is shifted.

To avoid having to work with a distinction of cases (LD vs. HD), a continuous function $\widehat{Y}^+$ is introduced:

$$\widehat{Y}^+ = \widehat{Y}^+_{\mathrm{LD}} W + \widehat{Y}^+_{\mathrm{HD}} (1 - W), \tag{16}$$

with

$$W = \frac{1}{1 + \exp\left(20\left(\tilde{s}_{\mathrm{conf}} - \tilde{s}^{\times}_{\mathrm{conf}}\right)\right)}, \tag{17}$$

where $W = 1$ for $\tilde{s}_{\mathrm{conf}} \ll \tilde{s}^{\times}_{\mathrm{conf}}$ and $W = 0$ for $\tilde{s}_{\mathrm{conf}} \gg \tilde{s}^{\times}_{\mathrm{conf}}$. The CE-scaled transport property $\widehat{Y}^+$ is a monovariate function of the reduced configurational entropy $\tilde{s}_{\mathrm{conf}}$ (cf. Fig. 3) in all state regions as shown below. Details of the framework are given in the Supplementary Material and an implementation is available on GitHub.

C. Component-Specific Correlation

CE-scaled transport properties are approximate monovariate functions of the configurational entropy $\tilde{s}_{\mathrm{conf}}$. Yet, the shape of this monovariate function is different for the three transport properties and for different components. The relation $\widehat{Y}^+(\tilde{s}_{\mathrm{conf}})$ is described here by an empirical, rational function

$$\left.\begin{matrix} \ln(\widehat{\eta}_i^+(\tilde{s}_{\mathrm{conf}})) \\ \widehat{\lambda}_i^+(\tilde{s}_{\mathrm{conf}}) \\ \ln(\widehat{D}_i^+(\tilde{s}_{\mathrm{conf}})) \end{matrix}\right\} = \frac{\alpha^{(Y)}_{0,i} + \alpha^{(Y)}_{\ln,i} \ln(\tilde{s}_{\mathrm{conf}} + 1) + \alpha^{(Y)}_{1,i} \tilde{s}_{\mathrm{conf}} + \alpha^{(Y)}_{2,i} (\tilde{s}_{\mathrm{conf}})^2 + \alpha^{(Y)}_{3,i} (\tilde{s}_{\mathrm{conf}})^3}{1 + g^{(Y)}_1 \ln(\tilde{s}_{\mathrm{conf}} + 1) + g^{(Y)}_2 \tilde{s}_{\mathrm{conf}}}. \tag{18}$$

The parameters $\alpha^{(Y)}_{0,i}$, $\alpha^{(Y)}_{\ln,i}$, $\alpha^{(Y)}_{1,i}$, $\alpha^{(Y)}_{2,i}$, and $\alpha^{(Y)}_{3,i}$ are specific for the studied component i as well as for the transport property Y. They are fitted for each substance to reference data. The number of parameters, i.e. terms, used in the nominator of Eq. (18) can be conveniently chosen for a given problem. The parameters $g^{(Y)}_1$ and $g^{(Y)}_2$ in the denominator are universal parameters for the transport property Y. All parameters of Eq. (18), i.e. $\alpha^{(Y)}_{0,i}$, $\alpha^{(Y)}_{\ln,i}$, $\alpha^{(Y)}_{1,i}$, $\alpha^{(Y)}_{2,i}$, $\alpha^{(Y)}_{3,i}$, $g^{(Y)}_1$, and $g^{(Y)}_2$, are dimensionless. The mathematical form (cf. Eq. (18)) and choice for the universal parameters (see below) provides well behaving functions for the resulting model, i.e. no pole for $\tilde{s}_{\mathrm{conf}} > 0$, and a defined limit for $\tilde{s}_{\mathrm{conf}} \to 0$, i.e. $\alpha^{(Y)}_{0,i}$.

D. Molecular Simulations and Adjustment of the Universal Parameters

The universal parameters, i.e. $g_1^{(Y)}$ and $g_2^{(Y)}$ (cf. Eq. (18)), were fitted to LJ simulation data. As suitable data were not available in the literature, homogeneous bulk phase MD simulations were carried out in this work with the software *ms*2[96,97]. The simulations were carried out for liquid, vapor, supercritical, metastable VLE and metastable solid-liquid equilibrium (SLE) regions as well as on the VLE binodal and the freezing line. In total, 173 state points were studied. The studied state points are depicted in Fig. 4.

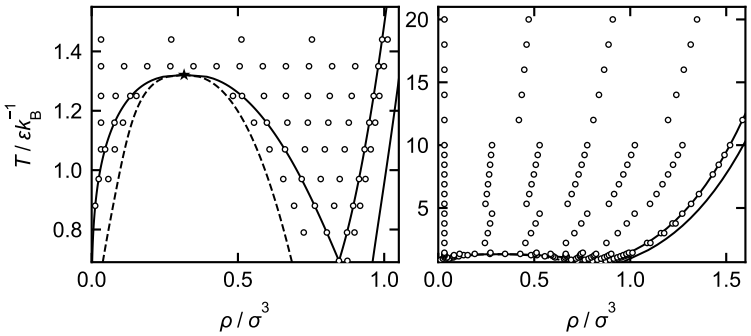

FIG. 4. Overview of the 173 state points (circles) of the LJ fluid that were studied in this work. The binodal and the critical point (star) were taken from Ref.[95], the spinodal from Ref.[98], and the freezing and melting lines from Ref.[99].

Each simulation consisted of 5000 particles. The gear predictor-corrector integrator was used with a time step of $\Delta t = 0.001 \left(\left(\sigma^2 M / N_A \right) / \varepsilon \right)^{1/2}$. The simulations were conducted in the NVT ensemble with 1×10^5 equilibration time steps and 5×10^6 production time steps. Periodic boundary conditions were applied in all directions. The viscosity, the thermal conductivity, and the self-diffusion coefficient were sampled using the *Green-Kubo*[100,101] formalism with a correlation length of 10^4 time steps for $\rho \geq 0.1\sigma^{-3}$ and 10^5 time steps for $\rho < 0.1\sigma^{-3}$. Details on the computational procedure of the *Green-Kubo* implementation in *ms*2 are given in Refs.[102,103]. The viscosity, the thermal conductivity, and the self-diffusion coefficient data obtained from the simulations were CE-scaled according to Eqs. (4) - (16). The second virial coefficient B of the LJ fluid and its derivative with respect to T used in Eqs. (8) - (10) were calculated analytically from the interaction potential[104]. Moreover, the configurational entropy was determined from the simulations. Therefore, the chemical potential μ_{conf} was sampled using *Widom*'s test particle method[105]. From that, the config-

urational *Helmholtz* energy a_{conf} was calculated as[96]

$$a_{\mathrm{conf}} = -\frac{\partial a_{\mathrm{conf}}}{\partial \rho}\rho + \mu_{\mathrm{conf}} = \frac{p}{\rho} + \mu_{\mathrm{conf}}. \tag{19}$$

The configurational entropy s_{conf} was then calculated as

$$s_{\mathrm{conf}} = \frac{u_{\mathrm{conf}}}{T} - \frac{a_{\mathrm{conf}}}{T}, \tag{20}$$

with u_{conf} being the configurational internal energy. Thereby, data for s_{conf}, $\widehat{\eta}^+$, $\widehat{\lambda}^+$, and $\widehat{D}^+$ of the LJ fluid were obtained in a wide state range. Details are discussed in the Supplementary Material. Moreover, the numeric data of the MD simulation results are provided in the electronic Supplementary Material.

The sampled entropy data were converted to the reduced configurational entropy $\tilde{s}_{\mathrm{conf}}$ using Eq. (7) and $m = 1$. The universal parameters $g_1^{(Y)}$ and $g_2^{(Y)}$ for the correlations for $Y \in \{\eta, \lambda, D\}$ (cf. Eq. (18)) were obtained from a fit to the computer experiment data $\widehat{\eta}^+(\tilde{s}_{\mathrm{conf}})$, $\widehat{\lambda}^+(\tilde{s}_{\mathrm{conf}})$, and $\widehat{D}^+(\tilde{s}_{\mathrm{conf}})$. The results are given in Table I.

TABLE I. Universal parameters of the entropy scaling framework, i.e. Eq. (18), as well as the component-specific parameters used for the fits of the universal parameters for the viscosity, the thermal conductivity, and the self-diffusion coefficient.

property	$f(\tilde{s}_{\mathrm{conf}})$	$g_1^{(Y)}$	$g_2^{(Y)}$	$\alpha_{0,\mathrm{LJ}}^{(Y)}$	$\alpha_{\mathrm{ln,LJ}}^{(Y)}$	$\alpha_{1,\mathrm{LJ}}^{(Y)}$	$\alpha_{2,\mathrm{LJ}}^{(Y)}$	$\alpha_{3,\mathrm{LJ}}^{(Y)}$
viscosity	$\ln(\widehat{\eta}^+(\tilde{s}_{\mathrm{conf}}))$	-1.6386	1.3923	0	0	0	1	0
thermal conductivity	$\widehat{\lambda}^+(\tilde{s}_{\mathrm{conf}})$	-1.9107	1.0725	1	0	0	0	1
self-diffusion	$\ln(\widehat{D}^+(\tilde{s}_{\mathrm{conf}}))$	0.6632	9.4714	0	0	0	0	-1

The component-specific parameters $\alpha_{0,\mathrm{LJ}}^{(Y)}$, $\alpha_{\mathrm{ln,LJ}}^{(Y)}$, $\alpha_{1,\mathrm{LJ}}^{(Y)}$, $\alpha_{2,\mathrm{LJ}}^{(Y)}$, and $\alpha_{3,\mathrm{LJ}}^{(Y)}$ were a priori fixed to constant values for the fit (see Table I). The value of $\alpha_{0,\mathrm{LJ}}^{(Y)}$ determines the low-density limit of the studied property, which is zero for $\ln(\widehat{\eta}^+)$ and $\ln(\widehat{D}^+)$ and 1 for $\widehat{\lambda}^+$. The logarithmic term and the linear term in the denominator of Eq. (18) were not used, i.e. $\alpha_{\mathrm{ln,LJ}}^{(Y)} = \alpha_{1,\mathrm{LJ}}^{(Y)} = 0$. The numbers for $\alpha_{2,\mathrm{LJ}}^{(Y)}$ and $\alpha_{3,\mathrm{LJ}}^{(Y)}$ were, depending on the property, set either to 0 or 1, so that the numerator of Eq. (18) is either a quadratic (viscosity) or a cubic function (thermal conductivity and self-diffusion coefficient) of the reduced configurational entropy $\tilde{s}_{\mathrm{conf}}$. As the denominator of Eq. (18) is linear, this results in a linear asymptote for $\tilde{s}_{\mathrm{conf}} \to \infty$ for the viscosity, which accounts for the approximately linear behavior of the CE-scaled viscosity

as function of the configurational entropy[24]. For the thermal conductivity and the self-diffusion coefficient, the CE-scaled transport properties can be described more accurately by a quadratic asymptote. The values for the parameters given in Table I are valid for the LJ fluid, but they can also be used as default and starting values for individual fits to data for other fluids. Fig. 5 shows the result of the fit for the CE-scaled properties as function of the reduced configurational entropy for the LJ fluid. The data are well represented by the fit.

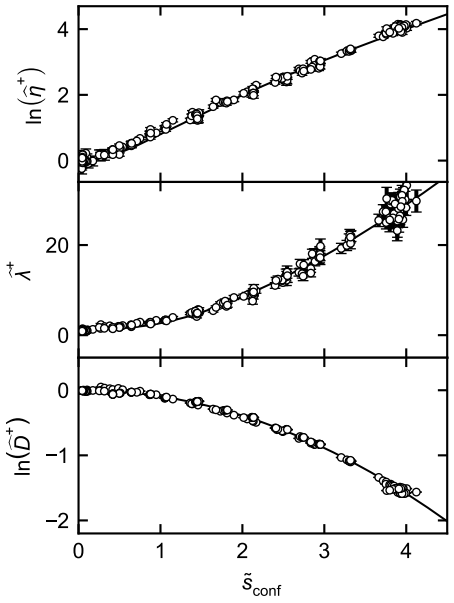

FIG. 5. CE-scaled viscosity $\widehat{\eta}^+$, thermal conductivity $\widehat{\lambda}^+$, and self-diffusion coefficient $\widehat{D}^+$ of the LJ fluid as function of the reduced configurational entropy $\tilde{s}_{\mathrm{conf}}$. Symbols represent MD simulation results (state points as shown in Fig. 4) and the solid line is the global fit to these results (cf. Eq. (18) and Table I). All shown properties are dimensionless.

The mean relative deviations of the fits are $\overline{\delta\widehat{\eta}^+} = 9.12\,\%$, $\overline{\delta\widehat{\lambda}^+} = 11.49\,\%$, and $\overline{\delta\widehat{D}^+} = 2.01\,\%$ and were calculated as

$$\overline{\delta Y} = \frac{1}{N_{\mathrm{exp}}} \sum_{j}^{N_{\mathrm{exp}}} \left|\delta Y_j\right| \tag{21}$$

$$\text{with} \quad \delta Y_j = \frac{Y_{\mathrm{exp},j} - Y_{\mathrm{ES},j}}{Y_{\mathrm{exp},j}}, \tag{22}$$

with N_{exp} being the number of data points, Y_{exp} the (computer) experiment value, and Y_{ES} the values obtained from the entropy scaling model. Since the studied state points cover a large range of states with respect to temperature and density (cf. Fig. 4), also a large

range of states with respect to the configurational entropy is covered (see Supplementary Material). For the viscosity and the thermal conductivity, the vast majority of the data points is described by the entropy scaling model with a deviation below 5 %; that number is 2 % for the self-diffusion coefficient. The deviations are larger for the data points at the largest configurational entropies which corresponds to very high densities, where the sampling of both the entropy and the transport properties is challenging. These deviations are of the same order as the relative statistical uncertainties of the simulation data for the viscosity and the thermal conductivity, which are on average 7.4 % and 8.5 %, respectively. For the self-diffusion coefficient, the corresponding uncertainty for the simulation data is 0.15 %.

Fig. 5 also indicates that the strategy proposed in the present work, that is based on different procedures for the LD region and the HD region, works well. The curves are smooth, also in the vicinity of the threshold at $\tilde{s}_{\mathrm{conf}} = 0.5$.

E. Extension to Mixtures

Also for mixtures, an approximately monovariate relation between the transport properties and the configurational entropy has been observed[40,88]. Therefore, the entropy scaling model for the viscosity and the thermal conductivity of pure components described above was extended to modeling mixture properties. The extension to self-diffusion coefficients is less straightforward, as there is one self-diffusion coefficient for each component, so this issue is not discussed here and left open for future work. In the approach, the mixture is treated as a pure pseudo-component following the one-fluid theory mixing rule concept[106,107].

Transport properties of mixtures are represented here as a function of the temperature, density, and composition $\underline{x}$, i.e. $Y_{\mathrm{mix}}(T, \rho, \underline{x})$, and described by the entropy scaling model as $\widehat{Y}^{+}_{\mathrm{mix}}(\tilde{s}_{\mathrm{conf}}(T, \rho, \underline{x}))$. In Eqs. (4) - (6), M is now the mean molar mass of the mixture

$$M = \sum_{i}^{N} x_i M_i, \tag{23}$$

where N is the number of components and x_i and M_i are the mole fraction and the molar mass of component i. The reduced configurational entropy of the mixture $\tilde{s}_{\mathrm{conf}}(T, \rho, \underline{x})$ is calculated from the molecular-based EOS using Eq. (7), where the segment number m of

the pseudo-component representing the mixture is calculated from

$$m = \sum_{i}^{N} x_i m_i, \tag{24}$$

where m_i is the segment number of the component i. The zero-density transport properties of the mixture were calculated as follows: the viscosity of the mixture in the zero-density limit $\eta^{+}_{\mathrm{CE,mix}}$ was calculated according to *Wilke*[108]

$$\begin{aligned} \eta^{+}_{\mathrm{CE,mix}} &= \sum_{i}^{N} \frac{x_i \eta^{+}_{\mathrm{CE},i}}{\sum_{j=1}^{N} x_i \phi_{ij}}, \\ \text{with} \quad \phi_{ij} &= \frac{\left(1 + (\eta^{+}_{\mathrm{CE},i}/\eta^{+}_{\mathrm{CE},j})^{1/2} (M_i/M_j)^{1/4}\right)^2}{\left(8(1 + M_i/M_j)\right)^{1/2}}, \end{aligned} \tag{25}$$

where $\eta^{+}_{\mathrm{CE},i}$ and $\eta^{+}_{\mathrm{CE},j}$ are the pure component *Chapman-Enskog* values for the viscosity (cf. Eq. (8)). The thermal conductivity of the mixture in the zero-density limit $\lambda^{+}_{\mathrm{CE,mix}}$ was calculated according to *Wassiljewa*[109] and *Mason* and *Saxena*[110] from

$$\begin{aligned} \lambda^{+}_{\mathrm{CE,mix}} &= \sum_{i}^{N} \frac{x_i \lambda^{+}_{\mathrm{CE},i}}{\sum_{j=1}^{N} x_i \phi_{ij}}, \\ \text{with} \quad \phi_{ij} &= \frac{\left(1 + (\lambda^{+}_{\mathrm{CE},i}/\lambda^{+}_{\mathrm{CE},j})^{1/2} (M_i/M_j)^{1/4}\right)^2}{\left(8(1 + M_i/M_j)\right)^{1/2}}, \end{aligned} \tag{26}$$

where $\lambda^{+}_{\mathrm{CE},i}$ and $\lambda^{+}_{\mathrm{CE},j}$ are the pure component *Chapman-Enskog* values for the thermal conductivity (cf. Eq. (9)). In Eq. (18), which describes the mathematical form of the generalized function $\widehat{Y}^{+}_{\mathrm{conf}}(\tilde{s}_{\mathrm{conf}})$, linear mixing rules are applied for the parameters, i.e.

$$\begin{aligned} \beta_{\mathrm{mix}} = \sum_{i}^{N} x_i \beta_i \quad \text{with} \quad & \beta_i \in \{\alpha^{(Y)}_{0,i}, \alpha^{(Y)}_{\mathrm{ln},i}, \alpha^{(Y)}_{1,i}, \alpha^{(Y)}_{2,i}, \alpha^{(Y)}_{3,i}\} \\ \text{and} \quad & \beta_{\mathrm{mix}} \in \{\alpha^{(Y)}_{0,\mathrm{mix}}, \alpha^{(Y)}_{\mathrm{ln,mix}}, \alpha^{(Y)}_{1,\mathrm{mix}}, \alpha^{(Y)}_{2,\mathrm{mix}}, \alpha^{(Y)}_{3,\mathrm{mix}}\}. \end{aligned} \tag{27}$$

Here, β_{mix} is the resulting parameter for the mixture, N is the number of components, x_i is the mole fraction of component i, and β_i indicates the component-specific parameters. The values for the universal parameters $g^{(Y)}_1$ and $g^{(Y)}_2$ (cf. Table I) are the same for pure components and mixtures. Additional information on the entropy scaling framework for mixtures is given in the Supplementary Material.

F. Remarks Regarding the Physical Basis of the Model Framework

The outlined entropy scaling framework is a physically-motivated model designed to be coupled with molecular-based EOS. The framework provides a basis for the modeling and prediction of transport properties in a wide range of thermodynamic states, different substance classes, and different EOS models (see applications below). Yet, the physical aspects of the entropy scaling model also comprise several assumptions and simplifications that influence the performance and are briefly critically summarized here. Moreover, while the entropy scaling framework is designed to be coupled with molecular-based EOS, it can in general be also used with empirical EOS. Yet, this route is not further exploited here.

In the zero-density limit, the *Chapman-Enskog* theory, which assumes spherical particles, is applied in our model. By applying the model, we assume that the *Chapman-Enskog* theory, coupled with the corresponding states principle, also works for more complex molecules. This is a relatively crude assumption for highly non-ideal fluids, e.g. H-bonding fluids. Furthermore, the thermal conductivity of gases depends on internal degrees of freedom, which are not considered in the *Chapman-Enskog* theory[93]. Hence, also the model developed in this work does not consider the influence of the internal degrees of freedom on the thermal conductivity[93], which can cause problems with predictions for fluids at low densities. However, fitting the parameter $\alpha_{0,i}^{(Y)}$ and not using the default value of 0 or 1 offers a pragmatic work-around that can alleviate some of these problems. More details are given in the applications section below and in the Supplementary Material. In principle, the framework proposed in this work could be extended by adding a model for the intramolecular degrees of freedom.

Furthermore, the smoothness of the transition between the LD and the HD region depends on the (presence of the) minimum of the function $Y_{\mathrm{CE}}^{+}(T)$, which depends on the description of the second virial coefficient by the employed EOS. In cases where the second virial coefficient is not described well by a given EOS, a work-around can be used – see Supplementary Material.

Moreover, in this work, molecular-based EOS with a classical scaling behavior were used such that systematic errors in the critical region have to be expected (overestimation of the critical temperature). The latter could be overcome by using more sophisticated EOS models, e.g. based on renormalization group theory[77], which were, however, not applied in

the present work.

Furthermore, the entropy scaling model itself does not account for near-critical effects, i.e. the critical enhancement[111]. In principle, additional contributions in the entropy scaling approach could be used to account for this, but we have refrained from considering this here, so that the model should not be used without modifications in the near-critical region.

III. APPLICATIONS

A. Overview

The new entropy scaling framework was applied in this work to pure substances and binary mixtures. To demonstrate the flexibility, different molecular-based EOS were used for the modeling. In total, 15 pure components, four binary mixtures, and a quaternary mixture were studied. Table II gives an overview of the studied pure components. Table III gives an overview of the studied mixtures. The results for the mixtures are predictions based on the pure component models (cf. Table II) and the mixing rules (cf. Eqs. (23) - (27)), i.e. they were obtained without any adjustment to experimental mixture data of transport properties. Also for the EOS mixture models, fully predictive mixing and combination rules were used.

Nine different molecular-based EOS were used to model the different substances (cf. Tables II and III). The choice of the EOS models was not optimized to create entropy scaling models with low deviations, but to show the general applicability and robustness of the framework. The individual choices were made so as to obtain examples that reflect realistic applications, e.g. the BACKONE EOS is often used for modeling refrigerants in the literature[115,116]. It was out of the scope of this work to compare the performance of different EOS. The EOS pure component parameters were adopted from the literature (see Supplementary Material for details). The entropy scaling parameters (cf. Eq. (18)) were fitted to transport property data taken from the literature. The number of parameters for each model (cf. Table II) was chosen so that no overfitting occurred for the function $\widehat{Y}^{+}(\tilde{s}_{\mathrm{conf}})$. For the viscosity, four parameters were used in most cases. For the thermal conductivity, five parameters were used since also the value $\alpha_{0,i}^{(\lambda)}$ had to be adjusted to get a good representation of the zero-density limit, for the reasons discussed in Section II F.

TABLE II. Overview of the studied pure components: the columns indicate (from left to right) the substance name, the EOS used for the modeling, the references for the pure component model. N_{exp} is the number of experimental data points used for the parameter adjustment and model evaluation, N_{par} the number of entropy scaling parameters used. $\overline{\delta Y}$ indicates the mean relative deviation (computed from Eq. (21)) for the viscosity η, the thermal conductivity λ, and the self-diffusion coefficient D.

substance	EOS	Ref.	viscosity			thermal conductivity			self-diffusion		
			N_{exp}	N_{par}	$\overline{\delta\eta}/\%$	N_{exp}	N_{par}	$\overline{\delta\lambda}/\%$	N_{exp}	N_{par}	$\overline{\delta D}/\%$
LJ	Kolafa-Nezbeda[81]	-	654	4	5.57	529	4	4.66	947	4	3.69
LJTS	PeTS[82]	-	348	4	4.54	348	4	3.91	348	2	5.22
methane	*Stephan* et al.[83]	112	2588	4	2.99	3082	5	5.84	318	4	5.53
n-butane	PC-SAFT[65]	65	973	4	4.36	2859	5	4.68	42	2	7.71
n-hexane	SAFT-VR Mie[84]	84	1487	4	3.36	1845	5	3.01	12	2	1.31
n-hexane[a]	SAFT-VR Mie[84]	84	867	4	3.18	-	-	-	-	-	
n-hexadecane	PC-SAFT[65]	65	592	4	5.7	431	3	1.81	109	2	8.63
propene	soft SAFT[85]	85	244	4	5.61	172	5	12.59	-	-	-
cyclohexane	PACT+B[70]	70	895	4	4.59	294	3	2.37	15	2	3
benzene	SAFT-VR Mie[84]	84	1379	4	3.63	803	5	2.93	426	2	4.02
nitrogen	SAFT-VR Mie[84]	89	2826	5	1.49	2223	5	2.86	-	-	-
carbon dioxide	PC-SAFT[65,90]	90	2911	4	2.82	1968	5	8.49	324	1	14.72
methanol	sCPA[73,86]	74	1233	5	3.84	609	5	4.81	103	3	4.78
1-propanol	SAFT-VR Mie[84]	84	896	2	5.44	273	5	4.82	-	-	-
1-octanol	PC-SAFT[65,113,114]	91	341	4	3.59	197	5	3.8	19	2	19.95
R134a	BACKONE[69]	69	742	4	3.71	6478	5	5.79	-	-	-

[a] extrapolation study (details below)

Only for the spherical model fluids (LJ and LJTS), the parameter $\alpha_{0,i}^{(\lambda)}$ was not fitted for the thermal conductivity due to the absence of internal degrees of freedom in this radial-symmetric model. For the self-diffusion coefficient, the data base is smaller for all substances. Except for the LJ fluid and methane, only one to three parameters were used in the entropy scaling model. All experimental data were used for adjusting the entropy scaling parameters,

TABLE III. Overview of the studied mixtures: the columns indicate (from left to right) the components, the EOS used for modeling, the *Berthelot* combination rule parameter ξ_{ij}, N_{exp} is the number of experimental data points used for the evaluation, $\overline{\delta Y}$ indicates the mean relative deviation (computed from Eq. (21)) for the viscosity η and the thermal conductivity λ. The size parameter σ was the same for both LJTS components, the pure component models for the other four (real) components were the same as in Table II. No parameters were adjusted to the mixture data.

components	EOS	ξ_{ij}	viscosity		thermal conductivity	
			N_{exp}	$\overline{\delta\eta}$/%	N_{exp}	$\overline{\delta\lambda}$/%
LJTS (ε_1) + LJTS ($\varepsilon_2 = 0.9\,\varepsilon_1$)	PeTS	1.2	55	4.71	55	5.42
LJTS (ε_1) + LJTS ($\varepsilon_2 = 0.9\,\varepsilon_1$)	PeTS	0.85	51	4.85	51	4.55
1-octanol + *n*-hexadecane	PC-SAFT	1	42	2.39	-	-
benzene + *n*-hexane	SAFT-VR Mie	1	-	-	19	3.47
n-decane + *n*-dodecane + *n*-tetradecane + *n*-hexadecane	PC-SAFT	1	18	1.97	-	-

except in the case of *n*-hexane modeled by the SAFT-VR Mie EOS (cf. Table II). To test the extrapolation capability of the model to states that were not considered in the fit, the model parameters for *n*-hexane were adjusted using state points $p \leq 10\,\text{MPa}$ alone. The model performance was then evaluated using data at $p > 10\,\text{MPa}$, which includes state points up to $p = 1000\,\text{MPa}$. Both the pure component EOS parameters and the entropy scaling parameters used in this work are reported in the Supplementary Material.

The experimental data for the real substances were taken from the Dortmund Database (DDB)[117] and from the database from *Suárez-Iglesias* et al.[118]. For the model fluids, i.e. the LJ and the Lennard-Jones truncated and shifted (LJTS) fluid, data were taken from Refs.[88,119–125]. Data from different fluid regions were considered for the entropy scaling modeling, i.e. gaseous, liquid, and supercritical (and in some cases also metastable) states in a large temperature and pressure range. In total, 43,750 data points were considered for the 15 pure components and 291 data points for the five mixtures. Overall, the availability of data on the transport properties of mixtures is significantly lower than that for the pure components. In all cases, the data compiled from the literature was screened for gross outliers

which were removed for the fit and model evaluation. Also, data in the direct vicinity of the critical point were omitted. The experimental data used in this work are given in the electronic Supplementary Material.

B. Pure Components

The mean relative deviation results for the pure components are given in Table II . They are in a range from 1.49 % to 19.95 %. For the vast majority of the studied pure components, a mean relative deviation below 6 % is obtained. This is impressive considering the fact that not more than five parameters were used for the fit that describes large data sets covering a wide range of conditions. Four typical examples are presented and discussed in detail in the main body of this paper, namely the viscosity of *n*-butane and *n*-hexane, the thermal conductivity of nitrogen, and the self-diffusion coefficient of benzene (cf. Table II). Details on the results for the other pure components are presented and discussed in the Supplementary Material.

Fig. 6 shows the entropy scaling plot $\widehat{Y}^+ = \widehat{Y}^+(\tilde{s}_{\mathrm{conf}})$ for the viscosity of *n*-butane, the thermal conductivity of nitrogen, and the self-diffusion coefficient of benzene (the corresponding plot for the viscosity of *n*-hexane is shown at the end of this chapter). In all three plots, the CE-scaled transport properties are distinct monovariate functions of the reduced configurational entropy in the entire range of $\tilde{s}_{\mathrm{conf}}$. The scattering of the data points is very small for all properties and substances. In all cases, a smooth transition between the LD and the HD region is observed.

In the following, the results for the four selected systems are discussed in detail by means of Figs. 7 - 10. For each example, the results from the entropy scaling model are compared to the reference data for selected isotherms (plot a in Figs. 7 - 10). Additionally, a deviation plot is shown (plot b in Figs. 7 - 10), which comprises all considered experimental data. Furthermore, a parity plot (plot e in Figs. 7 - 10) is given together with histograms of the temperature and pressure distributions of the considered state points (plots c and d in Figs. 7 - 10).

Fig. 7 shows the results for the viscosity of *n*-butane. Four parameters (cf. Eq. (18)) were adjusted to 973 experimental data points. The experimental data were in the range $0.0267\,\mathrm{MPa} < p < 1000\,\mathrm{MPa}$ and $140\,\mathrm{K} < T < 511\,\mathrm{K}$, which includes gaseous, liquid, as

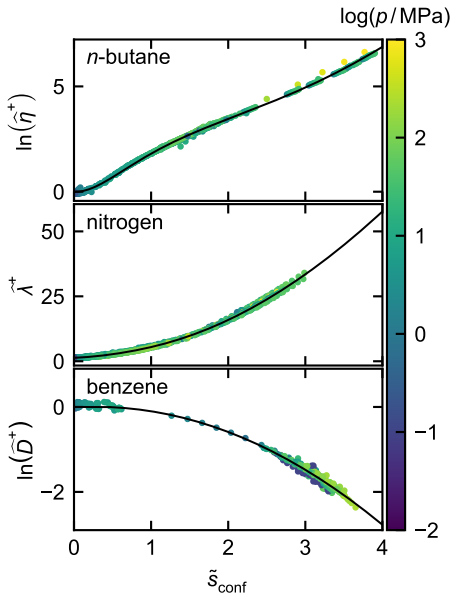

FIG. 6. CE-scaled viscosity $\widehat{\eta}^+$ of n-butane (top), CE-scaled thermal conductivity of nitrogen $\widehat{\lambda}^+$ (middle), and CE-scaled self-diffusion coefficient $\widehat{D}^+$ as function of the reduced configurational entropy $\tilde{s}_{\mathrm{conf}}$. Symbols are the data points derived from experimental data (η, λ, and D from experimental data and $\tilde{s}_{\mathrm{conf}}$ from the EOS). The EOS applied for the three substances are given in Table II. The color indicates the pressure. The black line is the entropy scaling model.

well as supercritical states. Most state points are in the temperature range from 300 to 500 K and pressure of 0.1 MPa to 100 MPa (cf. Fig. 7 c & d). The EOS was PC-SAFT. The viscosity of n-butane is described well by the model with a mean relative deviation of $\overline{\delta\eta} = 4.36\,\%$.

The supercritical isotherms cross each other in the vicinity of the critical point, which reflects the change of the temperature dependency. At low pressure, the viscosity increases with increasing temperature as predicted by the *Chapman-Enskog* theory; at high pressure at liquid-like states, the viscosity decreases with increasing temperature, which is as expected[19,93].

Overall, the entropy scaling model yields an excellent description of the viscosity over the whole temperature and pressure range. Only for pressures $p < 1\,\mathrm{MPa}$, the experimental values are slightly systematically overestimated by the entropy scaling model (cf. Fig. 7 b). This is due to an overestimation of the zero-density limit by the *Chapman-Enskog* theory in combination with the corresponding states principle.

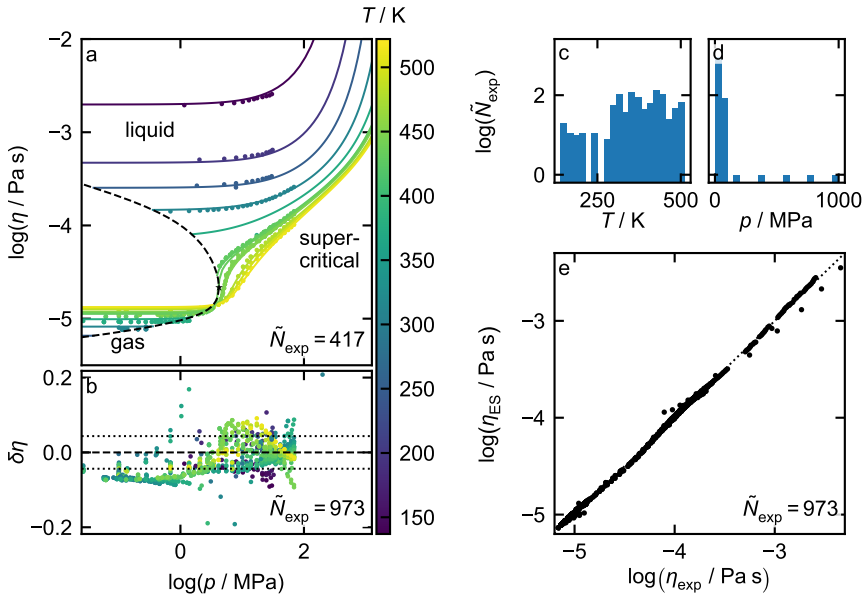

FIG. 7. Results for the viscosity η of n-butane. a: Viscosity η as function of the pressure p for 12 isotherms obtained from the entropy scaling model (lines) and experimental data (colored symbols). The viscosity computed from entropy scaling for the saturated liquid and saturated vapor (dashed line), and the critical point (star) are also given. b: Relative deviation between entropy scaling results and experimental data $\delta\eta$ (cf. Eq. (22)) as function of the pressure p (all considered data). The black dotted line indicates the mean average deviation $\overline{\delta\eta} = \pm 4.36\,\%$. a and b: The color indicates the temperature. c and d: Histograms of the number of experimental data points N_{exp} regarding their temperature (plot c) and pressure (plot d). e: Parity plot for the viscosity computed from the entropy scaling model η_{ES} vs. experimental data η_{exp} (all considered data). The entropy scaling results were obtained with the PC-SAFT EOS. $\tilde{N}_{exp}$ indicates the number of data points depicted in a given plot.

Fig. 8 shows the results for the thermal conductivity of nitrogen modeled by the entropy scaling model in conjunction with the SAFT-VR Mie EOS. The 2223 state points comprise temperatures in the range $77\,\mathrm{K} < T < 2473\,\mathrm{K}$ and pressures in the range $0.009\,\mathrm{MPa} < p < 1000\,\mathrm{MPa}$ (cf. Fig. 8 c & d), which includes a large amount of supercritical state points as well as some gas and few liquid state points. The structure of the $\lambda - \log(p)$ diagram regarding the different state regions (cf. Fig. 8 a) is similar to that for the viscosity. The isotherms with low temperatures are shown up to the solidification pressure (data taken

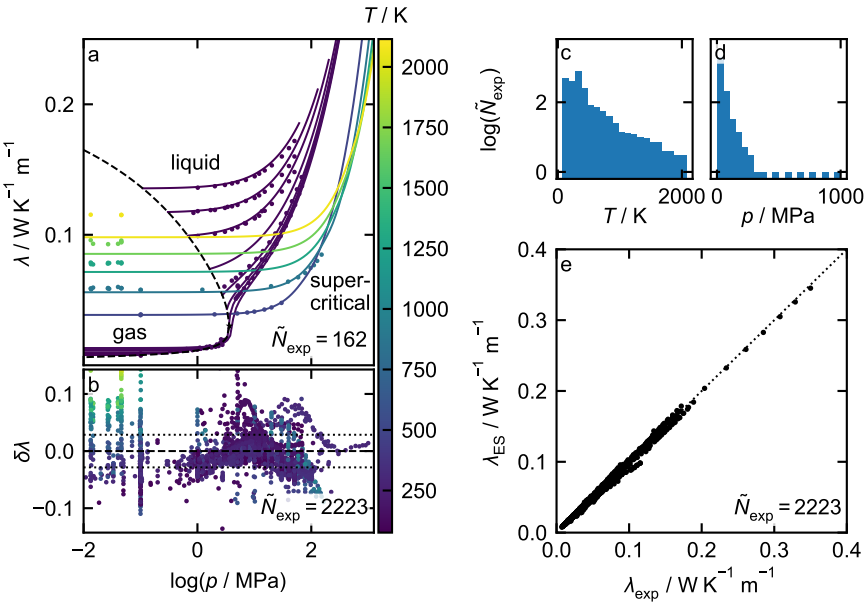

FIG. 8. Results for the thermal conductivity λ of nitrogen. a: Thermal conductivity λ as function of the pressure p for 13 isotherms obtained from the entropy scaling model (lines) and experimental data (colored symbols). The thermal conductivity computed from entropy scaling for the saturated liquid and saturated vapor (dashed line), and the critical point (star) are also given. b: Relative deviation between entropy scaling results and experimental data $\delta\lambda$ (cf. Eq. (22)) as function of the pressure p (all considered data). The black dotted line indicates the mean average deviation $\overline{\delta\lambda} = \pm 2.86\,\%$. a and b: The color indicates the temperature. c and d: Histograms of the number of experimental data points N_{exp} regarding their temperature (plot c) and pressure (plot d). e: Parity plot for the thermal conductivity computed from the entropy scaling model λ_{ES} vs. experimental data λ_{exp} (all considered data). The entropy scaling results were obtained with the SAFT-VR Mie EOS. $\tilde{N}_{exp}$ indicates the number of data points depicted in a given plot.

from *Grace* et al.[126]).

The mean relative deviation is $\overline{\delta\lambda} = 2.86\,\%$, which is impressive considering that only five parameters were fitted to a very large and diverse data set. Some larger deviations (up to $\delta\lambda = 15\,\%$) are observed in in the gas region at low pressure ($\log(p\,/\,\mathrm{MPa}) \leq -1$). These deviations slightly increase with increasing temperature. This is likely due to the fact that the *Chapman-Enskog* model does not consider internal degrees of freedom. On the other hand, state points at large pressures up to 1000 MPa and moderate temperatures

are described very well (cf. Fig. 8 b), i.e. with $\delta\lambda < 1.5\,\%$. These state points can also be identified in the parity plot (cf. Fig. 8 e) as the ones with $\lambda > 0.2\,\mathrm{W\,K^{-1}m^{-1}}$, which indicates the robustness of the macroscopic scaling used for dense states (cf. Eq. (16)).

Fig. 9 shows the results for the self-diffusion coefficient of benzene. Only two component-

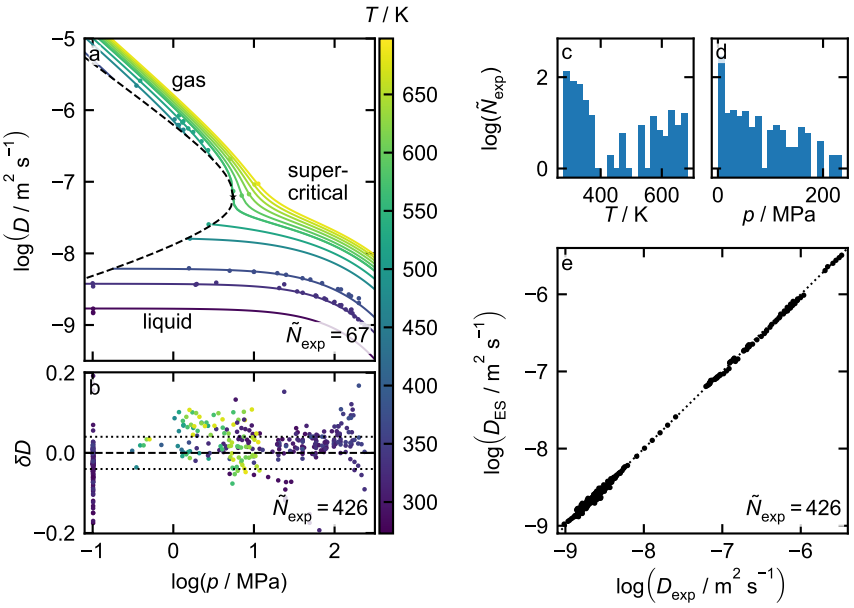

FIG. 9. Results for the self-diffusion coefficient D of benzene. a: Self-diffusion coefficient D as function of the pressure p for 12 isotherms obtained from the entropy scaling model (lines) and experimental data (colored symbols). The self-diffusion coefficient computed from entropy scaling for the saturated liquid and saturated vapor (dashed line), and the critical point (star) are also given. b: Relative deviation between entropy scaling results and experimental data δD (cf. Eq. (22)) as function of the pressure p (all considered data). The black dotted line indicates the mean average deviation $\overline{\delta D} = \pm 4.02\,\%$. a and b: The color indicates the temperature. c and d: Histograms of the number of experimental data points N_{exp} regarding their temperature (plot c) and pressure (plot d). e: Parity plot for the self-diffusion coefficient computed from the entropy scaling model D_{ES} vs. experimental data D_{exp} (all considered data). The entropy scaling results were obtained with the SAFT-VR Mie EOS. $\tilde{N}_{\mathrm{exp}}$ indicates the number of data points depicted in a given plot.

specific parameters were used. The experimental data of the self-diffusion coefficient for benzene ($N_{\mathrm{exp}} = 426$) cover temperatures in the range $279\,\mathrm{K} < T < 684\,\mathrm{K}$ and pressures in

the range 0.1 MPa $\leq p <$ 236 MPa, which corresponds to liquid, gaseous, and supercritical states. The majority of the data points is at temperatures below 373.15 K and ambient pressure, i.e. liquid states. The parity plot (cf. Fig. 9 e) reveals two groups of points, for liquid-like states ($D < 10^{-8}$ m^{2}s^{-1}) and for gas-like states ($D \geq 10^{-7}$ m^{2}s^{-1}). This distribution of the state points makes benzene an interesting candidate for testing the entropy scaling framework. The self-diffusion coefficient exhibits a qualitatively different behavior $D = D(p, T)$ compared to the viscosity and thermal conductivity. For all fluid states, D increases with increasing temperature and decreases with increasing pressure.

The self-diffusion coefficient of benzene is described with a mean average deviation of $\overline{\delta D} = 4.02\,\%$. This is impressive considering the fact that only two adjustable parameters were used. The description of the different state regions is overall similar. Hence, no region shows particularly high deviations, which indicates that the splitting approach between the low-density and high-density states in the entropy scaling framework works well. This is supported by the fact that also the gaseous state points at high temperatures $T > 550$ K are well described by the model.

Fig. 10 shows the results for the viscosity of *n*-hexane. Here, a different fitting strategy was used in order to test the extrapolation behavior of the entropy scaling framework: the experimental data were divided into two sets based on the pressure, state points at $p \leq$ 10 MPa were used for fitting the component-specific parameters of the entropy scaling model; state points at $p >$ 10 MPa were used for the assessment of the predictions of the entropy scaling model. Accordingly, 867 experimental state points were used for the parametrization and 620 state points were used for the evaluation of the predictions (cf. Table II). For *n*-hexane, all considered experimental data points for the assessment of the entropy scaling model are at supercritical pressure (up to 1000 MPa), but sub- and supercritical isotherms are shown, cf. Fig. 10 (the critical temperature and pressure are $T_c = 507.6$ K and $p_c = 3.02$ MPa[127], respectively). Four component-specific parameters were used in the fit. The entropy scaling model describes the data used for the fit ($p <$ 10 MPa) very well with a mean relative deviation of $\overline{\delta\eta} = 3.18\,\%$. Upon using the entropy scaling model for extrapolation ($p >$ 10 MPa), a mean relative deviation of $\overline{\delta\eta} = 2.88\,\%$ is obtained. The vast majority of predicted data points yields a deviation well below 10 %. For the data points at $p >$ 500 MPa (where also experiments are challenging to carry out), a larger deviation up to 38 % is obtained. Yet, the trends are qualitatively captured well at these extreme pressures. Hence,

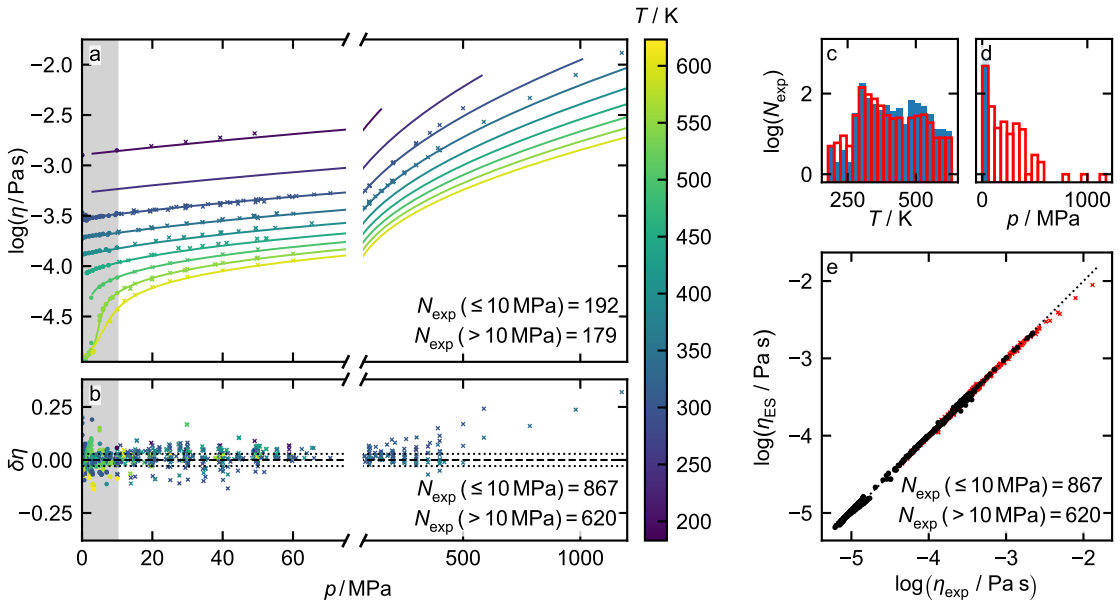

FIG. 10. Results for the viscosity η of n-hexane. a: Viscosity η as function of the pressure p for 9 isotherms computed from the entropy scaling model (lines) and experimental data (symbols). b: Relative deviation between entropy scaling model and experimental data $\delta\eta$ as function of the pressure p (all available experimental data). The black dotted line indicates the mean average deviation $\overline{\delta\eta}$ = ±3.18 %. a and b: The circles denote the data points at $p \leq 10$ MPa (grey area, used for fitting) and the crosses the data points at $p > 10$ MPa. The color indicates the temperature. c and d: Histograms of the number of experimental data points N_{exp} (blue: used for fit ($p \leq 10$ MPa), red: data points at $p > 10$ MPa) regarding their temperature (plot c) and pressure (plot d). e: Parity plot for the viscosity computed by the entropy scaling model η_{ES} vs. experimental data η_{exp} (black circles: state points used for fit ($p \leq 10$ MPa), red crosses: data points at $p > 10$ MPa). The entropy scaling results were obtained with the SAFT-VR Mie EOS. $\tilde{N}_{\text{exp}}$ indicates the number of data points depicted in a given plot.

the entropy scaling model is capable of making reliable predictions for the viscosity across two orders of magnitude in the pressure. Also the temperature dependency is very well described by the model.

The main reasons for the robust extrapolation behavior of the framework lie in the robust extrapolation behavior of the molecular-based EOS and the basic principle of the entropy scaling concept – correlating transport coefficients that are in general a function of two state

variables, e.g. T and p, by only the configurational entropy s_{conf} (which is a function of T and p in our example). This leads to situations, where an extrapolation in the T, p space is an interpolation in the $\tilde{s}_{\mathrm{conf}}$ space. This is illustrated in Fig. 11 for the n-hexane case discussed above. It shows the CE-scaled viscosity $\widehat{\eta}^{+}$ as function of the reduced configurational entropy

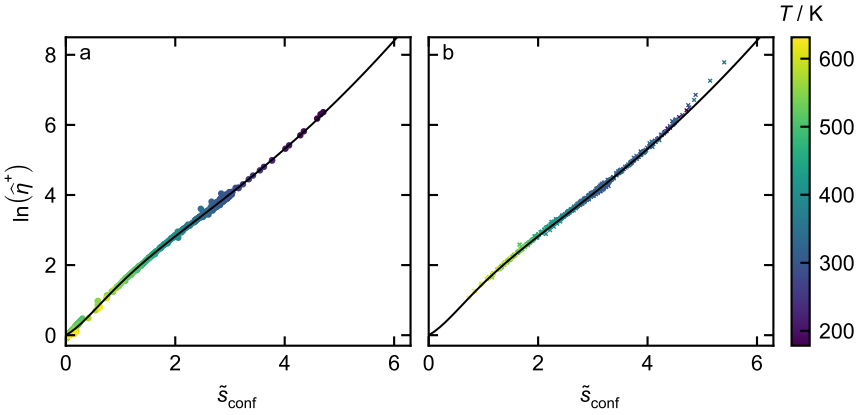

FIG. 11. CE-scaled viscosity $\widehat{\eta}^{+}$ as function of the reduced configurational entropy $\tilde{s}_{\mathrm{conf}}$ for n-hexane. Symbols are data points derived from experimental data (η from experimental data and $\tilde{s}_{\mathrm{conf}}$ from the SAFT-VR Mie EOS). The color indicates the temperature. The black line is the entropy scaling model. a: Data points at $p \leq 10\,\mathrm{MPa}$ (used for fit). b: Data points at $p > 10\,\mathrm{MPa}$ (testing extrapolation behavior). Both $\widehat{\eta}^{+}$ and $\tilde{s}_{\mathrm{conf}}$ are dimensionless properties.

$\tilde{s}_{\mathrm{conf}}$. For all considered experimental data points, the configurational entropy was computed (cf. Eq. (3)) from the EOS. The data points considered for the entropy scaling model fit ($p < 10\,\mathrm{MPa}$) lie in the range $0 < \tilde{s}_{\mathrm{conf}} < 5$ (cf. Fig. 11 a). For the vast majority of the data points at $p > 10\,\mathrm{MPa}$, the reduced configurational entropy $\tilde{s}_{\mathrm{conf}}$ is also in the range $0 < \tilde{s}_{\mathrm{conf}} < 5$ (cf. Fig. 11 b). Hence, the vast majority of data points predicted by the model at high pressure $p > 10\,\mathrm{MPa}$ are actually interpolated by the kernel of the model, i.e. in the entropy space. Only few state points are in fact extrapolations in the $\tilde{s}_{\mathrm{conf}}$ space, which are the state points with large viscosities at extremely high pressure (cf. Fig. 10). This principle could be favorably used in the design of experiment for determining most useful data for the parametrization of entropy scaling models.

C. Mixtures

The entropy scaling framework was also used for predicting transport properties of mixtures based on the pure component models discussed above. Five mixtures were studied (cf. Table III). The results for three mixtures are presented and discussed in the main body of this work; the results for the other two mixtures are presented in the Supplementary Material. For all studied mixtures, no parameters were fitted to the experimental data of the mixtures, i.e. the mixture results are pure predictions.

Fig. 12 shows the results for the viscosity and the thermal conductivity of an LJTS model mixture with $\sigma_2 = \sigma_1$, $M_1 = M_2$, $\varepsilon_2 = 0.9\,\varepsilon_1$, and $\xi = 1.2$[88]. The PeTS EOS[82] was used

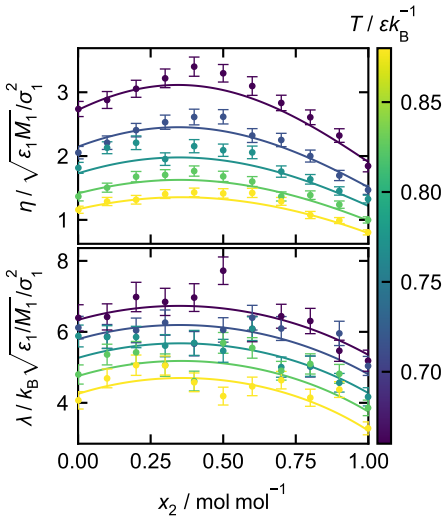

FIG. 12. Viscosity η (top) and thermal conductivity λ (bottom) of the LJTS mixture with $\sigma_2 = \sigma_1$, $\varepsilon_2 = 0.9\,\varepsilon_1$, and $\xi = 1.2$[88] as function of the mole fraction x_2. Molecular simulation data (symbols) from Ref.[88] and predictions with entropy scaling (lines). The color indicates the temperature. The pressure is $p = 0.1\,\varepsilon/\sigma^3$. The entropy scaling results were obtained with the PeTS EOS.

for modeling the LJTS mixtures. Results are shown for a wide temperature range and the entire composition range. The mixture exhibits a high-boiling azeotropic phase behavior for all studied temperatures[88]. All studied data points for the LJTS mixture are liquid phase state points. The predictions from the entropy scaling model are in excellent agreement with the reference data, which is astonishing considering the fact that the mixture is highly non-ideal. For all studied temperatures, both the viscosity and the thermal conductivity exhibit a maximum at $x_2 \approx 0.4\,\mathrm{mol\,mol^{-1}}$, which corresponds approximately to the azeotropic

composition[88]. For the vast majority of data points, the entropy scaling predictions agree with the computer experiment results within their uncertainties. The mean relative deviations of the entropy scaling model are $\overline{\delta\eta}$ = 4.71 % and $\overline{\delta\lambda}$ = 5.42 %. These deviations are even slightly below the mean relative deviations obtained for the pure LJTS component (cf. Table II) which emphasizes the predictive capabilities of the entropy scaling framework for modeling mixtures. The success of the predictions justifies the use of the simple linear mixing rules for the component-parameters of the fit function (cf. Eq. (18)) and emphasizes that the deviations from ideality are a result of the modeling of the entropy of the mixture by the EOS. The results for another LJTS mixture with same σ and ε values, but a mixing parameter ξ = 0.85 (cf. Table III), a mixture with a low-boiling azeotrope, are reported in the Supplementary Material. Also for this LJTS mixture, the performance of the entropy scaling framework is excellent.

Fig. 13 shows the results for the viscosity of the mixture 1-octanol + n-hexadecane. Predictions from the entropy scaling model are compared with experimental data for three

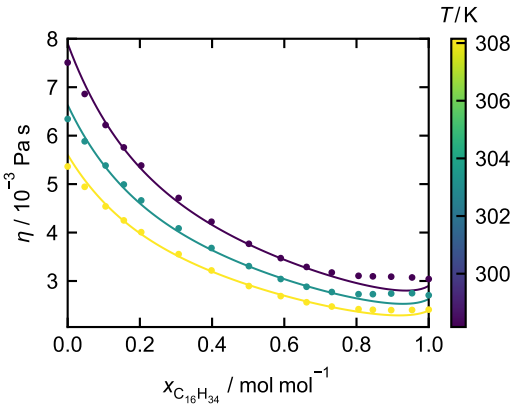

FIG. 13. Viscosity η of the mixture 1-octanol + n-hexadecane as function of the mole fraction of n-hexadecane $x_{C_{16}H_{34}}$ at ambient pressure p = 0.1 MPa. Experimental data[128] (symbols) and entropy scaling (lines). The color indicates the temperature. The entropy scaling results were obtained with the PC-SAFT EOS.

different temperatures from 298.15 K to 308.15 K at ambient pressure in the entire composition range. All considered state points are liquid. The predictions of the entropy scaling model are in excellent agreement with the experimental data. For mole fractions $x_{C_{16}H_{32}} \gtrsim 0.8\,\mathrm{mol\,mol^{-1}}$, the experimental viscosity data exhibit a plateau for all temperatures. The entropy scaling model predicts a faint minimum in that region. It is astonishing

that such details of the behavior are predicted by a model that was not trained to mixture data. Both the temperature and composition dependency of the viscosity are predicted well by the entropy scaling model. This is also reflected by the mean relative deviation of $\overline{\delta\eta} = 2.39\,\%$.

Fig. 14 shows the results for the quaternary mixture n-decane + n-dodecane + n-tetradecane + n-hexadecane. The predictions from entropy scaling are compared with

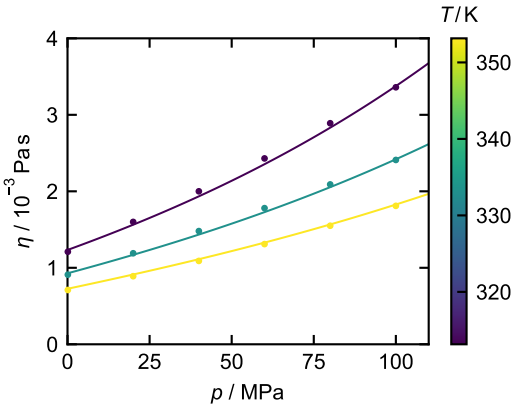

FIG. 14. Viscosity η of the mixture n-decane + n-dodecane + n-tetradecane + n-hexadecane as function of the pressure p with constant mole fractions $x_{C_{10}H_{22}} = 0.31\,\mathrm{mol\,mol^{-1}}$, $x_{C_{12}H_{26}} = 0.26\,\mathrm{mol\,mol^{-1}}$, $x_{C_{14}H_{30}} = 0.23\,\mathrm{mol\,mol^{-1}}$ and $x_{C_{16}H_{34}} = 0.20\,\mathrm{mol\,mol^{-1}}$. Experimental data[129] (symbols) and entropy scaling (lines). The color indicates the temperature. The entropy scaling results were obtained with the PC-SAFT EOS.

experimental data for three different temperatures (313.15 K, 333.15 K, and 353.15 K) as a function of the pressure. All considered state points are liquid. The entropy scaling model provides a very good description of the experimental data over the whole temperature and pressure range. Thus, the mean relative deviation is $\overline{\delta\eta} = 1.97\,\%$.

IV. CONCLUSIONS

An entropy scaling framework was developed for modeling transport properties of pure fluids and mixtures. The entropy scaling framework proposed in this work combines multiple physical theories and concepts such as the *Chapman-Enskog* theory, the *Rosenfeld* scaling theory, a LJ model at the kernel, the corresponding states principle, and molecular-based EOS. The aim of entropy scaling is to obtain a master curve that relates a suitably scaled

transport property to the configurational entropy of the studied fluid. In the entropy scaling framework proposed in this work, the *Rosenfeld* scaling is used for describing high-density states and the *Chapman-Enskog* theory for low-density states. The two approaches are connected in a convenient way using the lowest number obtained for the scaled zero-density limit from the *Chapman-Enskog* theory. This leads to a smooth transition between the scaled *Chapman-Enskog* data at low densities and the *Rosenfeld*-scaled data at high densities, which can be described easily as a function of the configurational entropy. The kernel of the entropy scaling framework comprises a LJ model such that the LJ critical parameters and the LJ collision integrals were adapted. We propose a generalized mathematical form for this master curve that contains both component-specific parameters as well as universal parameters. The latter were fitted in this work to transport data for the LJ fluid. The number of component-specific parameters can be varied, depending on the amount of available data. The mathematical form contains five component-specific parameters, but usually only some of these have to be adjusted to obtain good correlations of the available transport data of a given fluid. By applying simple mixing rules to these parameters, also transport properties of mixtures can be predicted from the pure component models. The applicability and good performance of this framework has been demonstrated in this work for several pure fluids and also for some mixtures.

Entropy scaling requires a suitable model for calculating the entropy, which is usually accomplished by an EOS. The entropy scaling framework proposed in this work is designed to be coupled with molecular-based EOS, which provide in many cases robust extrapolation capabilities to conditions not used in the model development. The EOS are integrated in the entropy scaling framework model in a consistent way by adapting the second virial coefficients, the critical point parameters, molecular property parameters, and the configurational entropy from the EOS. Based on that coupling, the entropy scaling framework can be flexibly used in conjunction with practically any molecular-based EOS (and in general also with empirical EOS). This was demonstrated by applying several molecular-based EOS, without, however, aiming at a systematic comparison of their performance.

The big advantage of combining entropy scaling with molecular-based EOS is that, based only on a few data points, transport properties can be predicted for a wide range of states. What may be a bold extrapolation in terms of the transport data in variables of temperature and pressure may turn out to be a simple interpolation in the scaled transport data as a

function of the configurational entropy.

Due to the strong physical basis of the framework, transport properties can be described in a large range of states with very few adjustable parameters. Even two parameters can provide a good description of transport property data in a wide state range. The entropy scaling framework was shown to yield excellent predictions also for states that were not considered for the parametrization, i.e. for metastable states, extreme pressure and temperature as well as for mixtures.

ACKNOWLEDGMENTS

The present research was conducted under the auspices of the Boltzmann-Zuse Society for Computational Molecular Engineering (BZS). The simulations were carried out on the Elwe at Regional University Computing Center Kaiserslautern-Landau (RHRZ) [Grant RPTU-MTD]. The project was funded by the Deutsche Forschungsgemeinschaft (DFG, German Research Foundation) - 252408385 - IRTG 2057, by the Federal Ministry of Education and Research (BMBF, Germany) - 16ME0613 - WindHPC, and by the KSB foundation - project 1354.

CREDIT AUTHORSHIP CONTRIBUTION STATEMENT

Sebastian Schmitt: Data Curation, Formal Analysis, Methodology (equal), Software (lead), Visualization, Writing/Original Draft Preparation (lead). **Hans Hasse:** Funding Acquisition (equal), Writing/Review & Editing (supporting). **Simon Stephan:** Conceptualization, Methodology (equal), Software (contributed), Supervision, Writing/Original Draft Preparation (supporting), Writing/Review & Editing (lead).

REFERENCES

[1]G. M. Kontogeorgis, R. Dohrn, I. G. Economou, J.-C. de Hemptinne, A. ten Kate, S. Kuitunen, M. Mooijer, L. F. ilnik, and V. Vesovic, "Industrial Requirements for Thermodynamic and Transport Properties: 2020," Industrial & Engineering Chemistry Research **60**, 4987–5013 (2021).

[2]G. W. Stachowiak and A. W. Batchelor, *Engineering tribology*, fourth edition ed. (Elsevier/Butterworth-Heinemann, Oxford, 2014).

[3]S. Stephan, S. Schmitt, H. Hasse, and H. M. Urbassek, "Molecular dynamics simulation of the Stribeck curve: Boundary lubrication, mixed lubrication, and hydrodynamic lubrication on the atomistic level," Friction **11**, 2342–2366 (2023).

[4]V. L. Popov, *Kontaktmechanik und Reibung: ein Lehr- und Anwendungsbuch von der Nanotribologie bis zur numerischen Simulation* (Springer, Berlin, 2009).

[5]S. Bair, "A Traction (Friction) Curve Is Not a Flow Curve," Lubricants **10**, 221 (2022).

[6]A. W. Islam and E. S. Carlson, "Viscosity Models and Effects of Dissolved CO_2," Energy & Fuels **26**, 5330–5336 (2012).

[7]H. O. Baled, I. K. Gamwo, R. M. Enick, and M. A. McHugh, "Viscosity models for pure hydrocarbons at extreme conditions: A review and comparative study," Fuel **218**, 89–111 (2018).

[8]L. C. Burrows, F. Haeri, P. Cvetic, S. Sanguinito, F. Shi, D. Tapriyal, A. Goodman, and R. M. Enick, "A Literature Review of CO_2, Natural Gas, and Water-Based Fluids for Enhanced Oil Recovery in Unconventional Reservoirs," Energy & Fuels **34**, 5331–5380 (2020).

[9]R. Krauss and K. Stephan, "Thermal Conductivity of Refrigerants in a Wide Range of Temperature and Pressure," Journal of Physical and Chemical Reference Data **18**, 43–76 (1989).

[10]B. L. Neindre and Y. Garrabos, "Transport Properties of Refrigerants," The Review of High Pressure Science and Technology **7**, 1183–1188 (1998).

[11]B. Kunstmann, I. Wlokas, M. Kohns, and H. Hasse, "Simulation study of superheating in evaporating droplets of (TTIP + p-xylene) in spray flame synthesis," Applications in Energy and Combustion Science **15**, 100156 (2023).

[12]F. Diewald, M. P. Lautenschlaeger, S. Stephan, K. Langenbach, C. Kuhn, S. Seckler, H.-J. Bungartz, H. Hasse, and R. Müller, "Molecular dynamics and phase field simulations of droplets on surfaces with wettability gradient," Computer Methods in Applied Mechanics and Engineering **361**, 112773 (2020).

[13]D. Schaefer, S. Stephan, K. Langenbach, M. T. Horsch, and H. Hasse, "Mass Transfer through Vapor-Liquid Interfaces Studied by Non-Stationary Molecular Dynamics Simulations," The Journal of Physical Chemistry B **127**, 2521–2533 (2023).

[14]R. A. Svehla, "Estimated Viscosities and Thermal Conductivities of Gases at High Temperatures," Technical Report NASA-TR-R-132 (Lewis Research Center, Cleveland, Ohio, 1962).

[15]E. Johannessen, J. Gross, and D. Bedeaux, "Nonequilibrium thermodynamics of interfaces using classical density functional theory," The Journal of Chemical Physics **129**, 184703 (2008).

[16]S. Schmitt, T. Vo, M. P. Lautenschlaeger, S. Stephan, and H. Hasse, "Molecular dynamics simulation study of heat transfer across solidfluid interfaces in a simple model system," Molecular Physics **120**, e2057364 (2022).

[17]M. P. Lautenschlaeger and H. Hasse, "Thermal, caloric and transport properties of the LennardJones truncated and shifted fluid in the adsorbed layers at dispersive solid walls," Molecular Physics **118**, 1–10 (2019).

[18]S. Stephan, D. Schaefer, K. Langenbach, and H. Hasse, "Mass transfer through vapour-liquid interfaces: a molecular dynamics simulation study," Molecular Physics **119**, e1810798 (2021).

[19]K. Stephan and K. Lucas, *Viscosity of Dense Fluids* (Springer US, Boston, MA, 1979).

[20]Y. Rosenfeld, "Relation between the transport coefficients and the internal entropy of simple systems," Physical Review A **15**, 2545–2549 (1977).

[21]Y. Rosenfeld, "A quasi-universal scaling law for atomic transport in simple fluids," Journal of Physics: Condensed Matter **11**, 5415–5427 (1999).

[22]J. C. Dyre, "Perspective: Excess-entropy scaling," The Journal of Chemical Physics **149**, 210901 (2018).

[23]J. Mairhofer, "A Residual Entropy Scaling Approach for Viscosity Based on the GERG-2008 Equation of State," Industrial & Engineering Chemistry Research **60**, 2652–2662 (2021).

[24]I. H. Bell, R. Messerly, M. Thol, L. Costigliola, and J. C. Dyre, "Modified Entropy Scaling of the Transport Properties of the Lennard-Jones Fluid," The Journal of Physical Chemistry B **123**, 6345–6363 (2019).

[25]I. H. Bell, "Entropy Scaling of ViscosityI: A Case Study of Propane," Journal of Chemical & Engineering Data **65**, 3203–3215 (2020).

[26]X. Yang, X. Xiao, E. F. May, and I. H. Bell, "Entropy Scaling of Viscosity - III: Application to Refrigerants and Their Mixtures," Journal of Chemical & Engineering Data **66**, 1385–1398 (2021).

[27]X. Yang, D. Kim, E. F. May, and I. H. Bell, "Entropy Scaling of Thermal Conductivity: Application to Refrigerants and Their Mixtures," Industrial & Engineering Chemistry Research **60**, 13052–13070 (2021).

[28]X. Li, K. Kang, Y. Gu, and X. Wang, "Viscosity prediction of pure refrigerants applying the residual entropy scaling theory coupled with a Generalized Chart parametrization method for the Statistical Associating Fluid Theory," Journal of Molecular Liquids **367**, 120479 (2022).

[29]A. Jäger, L. Steinberg, E. Mickoleit, and M. Thol, "Residual Entropy Scaling for Long-Chain Linear Alkanes and Isomers of Alkanes," Industrial & Engineering Chemistry Research **62**, 3767–3791 (2023).

[30]I. Nezbeda, "On Molecular-Based Equations of State: Perturbation Theories, Simple Models, and SAFT Modeling," Frontiers in Physics **8**, 1–17 (2020).

[31]E. A. Müller and K. E. Gubbins, "Molecular-Based Equations of State for Associating Fluids: A Review of SAFT and Related Approaches," Industrial & Engineering Chemistry Research **40**, 2193–2211 (2001).

[32]S. Stephan, K. Langenbach, and H. Hasse, "Interfacial properties of binary Lennard-Jones mixtures by molecular simulation and density gradient theory," The Journal of Chemical Physics **150**, 174704 (2019).

[33]T. Zeiner and S. Enders, "Phase behavior of hyperbranched polymer solutions in mixed solvents," Chemical Engineering Science **66**, 5244–5252 (2011).

[34]D. Fertig and S. Stephan, "Influence of dispersive long-range interactions on transport and excess properties of simple mixtures," Molecular Physics **0**, e2162993 (2023).

[35]"Phase equilibria of symmetric Lennard-Jones mixtures and a look at the transport properties near the upper critical solution temperature," **25**, 10.1039/D3CP01434G.

[36]O. Lobanova, A. Mejía, G. Jackson, and E. A. Müller, "SAFT- force field for the simulation of molecular fluids 6: Binary and ternary mixtures comprising water, carbon dioxide, and n -alkanes," The Journal of Chemical Thermodynamics **93**, 320–336 (2016).

[37]O. Lötgering-Lin and J. Gross, "Group Contribution Method for Viscosities Based on Entropy Scaling Using the Perturbed-Chain Polar Statistical Associating Fluid Theory," Industrial & Engineering Chemistry Research **54**, 7942–7952 (2015).

[38]M. Hopp and J. Gross, "Thermal Conductivity of Real Substances from Excess Entropy Scaling Using PCP-SAFT," Industrial & Engineering Chemistry Research **56**, 4527–4538 (2017).

[39]M. Hopp, J. Mele, and J. Gross, "Self-Diffusion Coefficients from Entropy Scaling Using the PCP-SAFT Equation of State," Industrial & Engineering Chemistry Research **57**, 12942–12950 (2018).

[40]O. Lötgering-Lin, M. Fischer, M. Hopp, and J. Gross, "Pure Substance and Mixture Viscosities Based on Entropy Scaling and an Analytic Equation of State," Industrial & Engineering Chemistry Research **57**, 4095–4114 (2018).

[41]M. Hopp, J. Mele, R. Hellmann, and J. Gross, "Thermal Conductivity via Entropy Scaling: An Approach That Captures the Effect of Intramolecular Degrees of Freedom," Industrial & Engineering Chemistry Research **58**, 18432–18438 (2019).

[42]M. Hopp and J. Gross, "Thermal Conductivity from Entropy Scaling: A Group-Contribution Method," Industrial & Engineering Chemistry Research **58**, 20441–20449 (2019).

[43]J. Zmpitas and J. Gross, "Modified StokesEinstein Equation for Molecular Self-Diffusion Based on Entropy Scaling," Industrial & Engineering Chemistry Research **60**, 4453–4459 (2021).

[44]L. T. Novak, "Fluid Viscosity-Residual Entropy Correlation," International Journal of Chemical Reactor Engineering **9**, 1–27 (2011).

[45]L. T. Novak, "Predictive Corresponding-States Viscosity Model for the Entire Fluid Region: n-Alkanes," Industrial & Engineering Chemistry Research **52**, 6841–6847 (2013).

[46]L. T. Novak, "Predicting Fluid Viscosity of Nonassociating Molecules," Industrial & Engineering Chemistry Research **54**, 5830–5835 (2015).

[47]A. Dehlouz, J.-N. Jaubert, G. Galliero, M. Bonnissel, and R. Privat, "Entropy Scaling-Based Correlation for Estimating the Self-Diffusion Coefficients of Pure Fluids," Industrial

& Engineering Chemistry Research **61**, 14033–14050 (2022).

[48]A. Dehlouz, J.-N. Jaubert, G. Galliero, M. Bonnissel, and R. Privat, "Combining the entropy-scaling concept and cubic- or SAFT equations of state for modelling thermal conductivities of pure fluids," International Journal of Heat and Mass Transfer **196**, 123286 (2022).

[49]A. Dehlouz, R. Privat, G. Galliero, M. Bonnissel, and J.-N. Jaubert, "Revisiting the Entropy-Scaling Concept for Shear-Viscosity Estimation from Cubic and SAFT Equations of State: Application to Pure Fluids in Gas, Liquid and Supercritical States," Industrial & Engineering Chemistry Research **60**, 12719–12739 (2021).

[50]W. A. Fouad and L. F. Vega, "Transport properties of HFC and HFO based refrigerants using an excess entropy scaling approach," The Journal of Supercritical Fluids **131**, 106–116 (2018).

[51]S. Stephan and U. K. Deiters, "Characteristic Curves of the Lennard-Jones Fluid," International Journal of Thermophysics **41**, 147 (2020).

[52]O. L. Boshkova and U. K. Deiters, "Soft Repulsion and the Behavior of Equations of State at High Pressures," International Journal of Thermophysics **31**, 227–252 (2010).

[53]L. Yelash, M. Müller, W. Paul, and K. Binder, "Artificial multiple criticality and phase equilibria: an investigation of the PC-SAFT approach," Physical Chemistry Chemical Physics **7**, 3728–3732 (2005).

[54]R. Privat, R. Gani, and J.-N. Jaubert, "Are safe results obtained when the PC-SAFT equation of state is applied to ordinary pure chemicals?" Fluid Phase Equilibria **295**, 76–92 (2010).

[55]I. H. Bell, "Entropy Scaling of ViscosityII: Predictive Scheme for Normal Alkanes," Journal of Chemical & Engineering Data **65**, 5606–5616 (2020).

[56]R. V. Vaz, A. L. Magalhães, D. L. A. Fernandes, and C. M. Silva, "Universal correlation of self-diffusion coefficients of model and real fluids based on residual entropy scaling law," Chemical Engineering Science **79**, 153–162 (2012).

[57]T. Nguyen, S. Khennache, G. Galliero, T. Tran, L. Tuong, P. Nguyen, H. Hoang, and H. K. Ho, "Entropy Scaling for Viscosity of Pure Lennard-Jones Fluids and Their Binary Mixtures," Communications in Physics **32**, 187–200 (2022).

[58]W. P. Krekelberg, M. J. Pond, G. Goel, V. K. Shen, J. R. Errington, and T. M. Truskett, "Generalized Rosenfeld scalings for tracer diffusivities in not-so-simple fluids: Mixtures

and soft particles," Physical Review E **80**, 061205 (2009).

[59]S. Pieprzyk, D. M. Heyes, and A. C. Braka, "Thermodynamic properties and entropy scaling law for diffusivity in soft spheres," Physical Review E **90**, 012106 (2014).

[60]N. Gnan, T. B. Schrøder, U. R. Pedersen, N. P. Bailey, and J. C. Dyre, "Pressure-energy correlations in liquids. IV. Isomorphs in liquid phase diagrams," The Journal of Chemical Physics **131**, 234504 (2009).

[61]T. B. Schrøder, N. Gnan, U. R. Pedersen, N. P. Bailey, and J. C. Dyre, "Pressure-energy correlations in liquids. V. Isomorphs in generalized Lennard-Jones systems," The Journal of Chemical Physics **134**, 164505 (2011).

[62]I. H. Bell, "Probing the link between residual entropy and viscosity of molecular fluids and model potentials," Proceedings of the National Academy of Sciences **116**, 4070–4079 (2019).

[63]R. Span, *Multiparameter Equations of State* (Springer Berlin Heidelberg, Berlin, Heidelberg, 2000).

[64]W. Chapman, K. Gubbins, G. Jackson, and M. Radosz, "SAFT: Equation-of-state solution model for associating fluids," Fluid Phase Equilibria **52**, 31–38 (1989).

[65]J. Gross and G. Sadowski, "Perturbed-Chain SAFT: An Equation of State Based on a Perturbation Theory for Chain Molecules," Industrial & Engineering Chemistry Research **40**, 1244–1260 (2001).

[66]Y. Zhang and W. G. Chapman, "Modeling Thermodynamic Properties of Isomeric Alkanes with a New Branched Equation of State," Industrial & Engineering Chemistry Research **57**, 1679–1688 (2018).

[67]I. G. Economou, "Statistical Associating Fluid Theory: A Successful Model for the Calculation of Thermodynamic and Phase Equilibrium Properties of Complex Fluid Mixtures," Industrial & Engineering Chemistry Research **41**, 953–962 (2002).

[68]A. Müller, J. Winkelmann, and J. Fischer, "Backone family of equations of state: 1. Nonpolar and polar pure fluids," AIChE Journal **42**, 1116–1126 (1996).

[69]U. Weingerl, M. Wendland, J. Fischer, A. Müller, and J. Winkelmann, "Backone family of equations of state: 2. Nonpolar and polar fluid mixtures," AIChE Journal **47**, 705–717 (2001).

[70]R. L. Cotterman, B. J. Schwarz, and J. M. Prausnitz, "Molecular thermodynamics for fluids at low and high densities. Part I: Pure fluids containing small or large molecules,"

AIChE Journal **32**, 1787–1798 (1986).

[71]R. L. Cotterman and J. M. Prausnitz, "Molecular thermodynamics for fluids at low and high densities. Part II: Phase equilibria for mixtures containing components with large differences in molecular size or potential energy," AIChE Journal **32**, 1799–1812 (1986).

[72]W. G. Chapman, K. E. Gubbins, G. Jackson, and M. Radosz, "New reference equation of state for associating liquids," Industrial & Engineering Chemistry Research **29**, 1709–1721 (1990).

[73]G. M. Kontogeorgis, E. C. Voutsas, I. V. Yakoumis, and D. P. Tassios, "An Equation of State for Associating Fluids," Industrial & Engineering Chemistry Research **35**, 4310–4318 (1996).

[74]G. M. Kontogeorgis, M. L. Michelsen, G. K. Folas, S. Derawi, N. Von Solms, and E. H. Stenby, "Ten Years with the CPA (Cubic-Plus-Association) Equation of State. Part 1. Pure Compounds and Self-Associating Systems," Industrial & Engineering Chemistry Research **45**, 4855–4868 (2006).

[75]J. Staubach and S. Stephan, "Prediction of Thermodynamic Properties of Fluids at Extreme Conditions: Assessment of the Consistency of Molecular-Based Models," in *Proceedings of the 3rd Conference on Physical Modeling for Virtual Manufacturing Systems and Processes*, edited by J. C. Aurich, C. Garth, and B. S. Linke (Springer International Publishing, Cham, 2023) pp. 170–188.

[76]M. Urschel and S. Stephan, "Determining Browns Characteristic Curves Using Molecular Simulation," Journal of Chemical Theory and Computation **19**, 1537–1552 (2023).

[77]J. A. White and S. Zhang, "Renormalization group theory for fluids," The Journal of Chemical Physics **99**, 2012–2019 (1993).

[78]J. S. Rowlinson and F. L. Swinton, *Liquids and Liquid Mixtures: Butterworths monographs in chemistry* (Butterworth-Heinemann, Oxford, England, 2013).

[79]S. Stephan and H. Hasse, "Molecular interactions at vapor-liquid interfaces: Binary mixtures of simple fluids," Physical Review E **101**, 012802 (2020).

[80]D. Berthelot, "Sur le melange des gaz," Comptes rendus hebdomadaires des séances de l'Académie des sciences **126**, 1703 – 1706 (1898).

[81]J. Kolafa and I. Nezbeda, "The Lennard-Jones fluid: an accurate analytic and theoretically-based equation of state," Fluid Phase Equilibria **100**, 1–34 (1994).

[82]M. Heier, S. Stephan, J. Liu, W. G. Chapman, H. Hasse, and K. Langenbach, "Equation of state for the Lennard-Jones truncated and shifted fluid with a cut-off radius of 2.5 σ based on perturbation theory and its applications to interfacial thermodynamics," Molecular Physics **116**, 2083–2094 (2018).

[83]S. Stephan, J. Staubach, and H. Hasse, "Review and comparison of equations of state for the Lennard-Jones fluid," Fluid Phase Equilibria **523**, 112772 (2020).

[84]T. Lafitte, A. Apostolakou, C. Avendaño, A. Galindo, C. S. Adjiman, E. A. Müller, and G. Jackson, "Accurate statistical associating fluid theory for chain molecules formed from Mie segments," The Journal of Chemical Physics **139**, 154504 (2013).

[85]F. J. Blas and L. F. Vega, "Prediction of Binary and Ternary Diagrams Using the Statistical Associating Fluid Theory (SAFT) Equation of State," Industrial & Engineering Chemistry Research **37**, 660–674 (1998).

[86]G. M. Kontogeorgis, I. V. Yakoumis, H. Meijer, E. Hendriks, and T. Moorwood, "Multicomponent phase equilibrium calculations for watermethanolalkane mixtures," Fluid Phase Equilibria **158-160**, 201–209 (1999).

[87]S. Stephan, M. T. Horsch, J. Vrabec, and H. Hasse, "MolMod an open access database of force fields for molecular simulations of fluids," Molecular Simulation **45**, 806–814 (2019).

[88]D. Fertig, H. Hasse, and S. Stephan, "Transport properties of binary Lennard-Jones mixtures: Insights from entropy scaling and conformal solution theory," Journal of Molecular Liquids **367**, 120401 (2022).

[89]A. Gonzalez, L. Pereira, P. Paricaud, C. Coquelet, and A. Chapoy, "Modeling of Transport Properties Using the SAFT-VR Mie Equation of State," in *SPE Annual Technical Conference and Exhibition* (SPE, Houston, Texas, USA, 2015) p. D031S043R005.

[90]J. Gross, "An equation-of-state contribution for polar components: Quadrupolar molecules," AIChE Journal **51**, 2556–2568 (2005).

[91]N. M. Al-Saifi, E. Z. Hamad, and P. Englezos, "Prediction of vaporliquid equilibrium in wateralcoholhydrocarbon systems with the dipolar perturbed-chain SAFT equation of state," Fluid Phase Equilibria **271**, 82–93 (2008).

[92]I. H. Bell, R. Hellmann, and A. H. Harvey, "Zero-Density Limit of the Residual Entropy Scaling of Transport Properties," Journal of Chemical & Engineering Data **65**, 1038–1050 (2020).

[93]B. E. Poling, J. M. Prausnitz, and J. P. O'Connell, *The properties of gases and liquids*, 5th ed. (McGraw-Hill, New York, 2001).

[94]S. U. Kim and C. W. Monroe, "High-accuracy calculations of sixteen collision integrals for Lennard-Jones (126) gases and their interpolation to parameterize neon, argon, and krypton," Journal of Computational Physics **273**, 358–373 (2014).

[95]S. Stephan, M. Thol, J. Vrabec, and H. Hasse, "Thermophysical Properties of the Lennard-Jones Fluid: Database and Data Assessment," Journal of Chemical Information and Modeling **59**, 4248–4265 (2019).

[96]R. Fingerhut, G. Guevara-Carrion, I. Nitzke, D. Saric, J. Marx, K. Langenbach, S. Prokopev, D. Celný, M. Bernreuther, S. Stephan, M. Kohns, H. Hasse, and J. Vrabec, "ms2: A molecular simulation tool for thermodynamic properties, release 4.0," Computer Physics Communications **262**, 107860 (2021).

[97]G. Rutkai, A. Köster, G. Guevara-Carrion, T. Janzen, M. Schappals, C. W. Glass, M. Bernreuther, A. Wafai, S. Stephan, M. Kohns, S. Reiser, S. Deublein, M. Horsch, H. Hasse, and J. Vrabec, "ms2: A molecular simulation tool for thermodynamic properties, release 3.0," Computer Physics Communications **221**, 343–351 (2017).

[98]M. Thol, G. Rutkai, A. Köster, R. Lustig, R. Span, and J. Vrabec, "Equation of State for the Lennard-Jones Fluid," Journal of Physical and Chemical Reference Data **45**, 023101 (2016).

[99]A. J. Schultz and D. A. Kofke, "Comprehensive high-precision high-accuracy equation of state and coexistence properties for classical Lennard-Jones crystals and low-temperature fluid phases," The Journal of Chemical Physics **149**, 204508 (2018).

[100]M. S. Green, "Markoff Random Processes and the Statistical Mechanics of TimeDependent Phenomena. II. Irreversible Processes in Fluids," The Journal of Chemical Physics **22**, 398–413 (1954).

[101]R. Kubo, "Statistical-Mechanical Theory of Irreversible Processes. I. General Theory and Simple Applications to Magnetic and Conduction Problems," Journal of the Physical Society of Japan **12**, 570–586 (1957).

[102]S. Deublein, B. Eckl, J. Stoll, S. V. Lishchuk, G. Guevara-Carrion, C. W. Glass, T. Merker, M. Bernreuther, H. Hasse, and J. Vrabec, "ms2: A molecular simulation tool for thermodynamic properties," Computer Physics Communications **182**, 2350–2367 (2011).

[103]C. W. Glass, S. Reiser, G. Rutkai, S. Deublein, A. Köster, G. Guevara-Carrion, A. Wafai, M. Horsch, M. Bernreuther, T. Windmann, H. Hasse, and J. Vrabec, "ms2: A molecular simulation tool for thermodynamic properties, new version release," Computer Physics Communications **185**, 3302–3306 (2014).

[104]P. Vargas, E. Munoz, and L. Rodriguez, "Second virial coe cient for the LennardJones potential," Physica A (2001).

[105]B. Widom, "Some Topics in the Theory of Fluids," The Journal of Chemical Physics **39**, 2808–2812 (1963).

[106]U. K. Deiters and T. Kraska, *High-pressure fluid phase equilibria: phenomenology and computation*, Supercritical fluid science and technology No. v. 2 (Elsevier, Amsterdam ; Boston, 2012).

[107]J.-P. Hansen and I. R. McDonald, *Theory of simple liquids: with applications of soft matter*, fourth edition ed. (Elsevier/AP, Amstersdam, 2013).

[108]C. R. Wilke, "A Viscosity Equation for Gas Mixtures," The Journal of Chemical Physics **18**, 517–519 (1950).

[109]A. Wassiljewa, "Wärmeleitung in Gasgemischen," Physikalische Zeitschrift **5**, 737 (1904).

[110]E. A. Mason and S. C. Saxena, "Approximate Formula for the Thermal Conductivity of Gas Mixtures," The Physics of Fluids **1**, 361–369 (1958).

[111]J. V. Sengers, "Transport properties of fluids near critical points," International Journal of Thermophysics **6**, 203–232 (1985).

[112]J. Vrabec, J. Stoll, and H. Hasse, "A Set of Molecular Models for Symmetric Quadrupolar Fluids," The Journal of Physical Chemistry B **105**, 12126–12133 (2001).

[113]J. Gross and G. Sadowski, "Application of the Perturbed-Chain SAFT Equation of State to Associating Systems," Industrial & Engineering Chemistry Research **41**, 5510–5515 (2002).

[114]J. Gross and J. Vrabec, "An equation-of-state contribution for polar components: Dipolar molecules," AIChE Journal **52**, 1194–1204 (2006).

[115]N. A. Lai and T. T. H. Phan, "Review of the BACKONE equation of state and its applications," Molecular Physics **115**, 1041–1050 (2017).

[116]B. Saleh, G. Koglbauer, M. Wendland, and J. Fischer, "Working fluids for low-temperature organic Rankine cycles," Energy **32**, 1210–1221 (2007).

[117]"Dortmund Data Bank, 2023, www.ddbst.com,".

[118]O. Suárez-Iglesias, I. Medina, M. Sanz, C. Pizarro, and J. L. Bueno, "Self-Diffusion in Molecular Fluids and Noble Gases: Available Data," Journal of Chemical & Engineering Data **60**, 2757–2817 (2015).

[119]V. G. Baidakov, S. P. Protsenko, and Z. R. Kozlova, "Metastable Lennard-Jones fluids. I. Shear viscosity," The Journal of Chemical Physics **137**, 164507 (2012).

[120]D. M. Heyes, "Transport coefficients of Lennard-Jones fluids: A molecular-dynamics and effective-hard-sphere treatment," Physical Review B **37**, 5677–5696 (1988).

[121]J. C. Thomas and R. L. Rowley, "Transient molecular dynamics simulations of viscosity for simple fluids," The Journal of Chemical Physics **127**, 174510 (2007).

[122]V. G. Baidakov and S. P. Protsenko, "Metastable Lennard-Jones fluids. II. Thermal conductivity," The Journal of Chemical Physics **140**, 214506 (2014).

[123]M. Bugel and G. Galliero, "Thermal Conductivity of the Lennard-Jones Fluid: An Empirical Correlation," Chemical Physics **352**, 249–257 (2008).

[124]V. G. Baidakov, S. P. Protsenko, and Z. R. Kozlova, "The self-diffusion coefficient in stable and metastable states of the LennardJones fluid," Fluid Phase Equilibria **305**, 106–113 (2011).

[125]K. Meier, A. Laesecke, and S. Kabelac, "Transport coefficients of the Lennard-Jones model fluid. II Self-diffusion," The Journal of Chemical Physics **121**, 9526–9535 (2004).

[126]J. Grace and G. Kennedy, "The melting curve of five gases to 30 kb," Journal of Physics and Chemistry of Solids **28**, 977–982 (1967).

[127]P. Linstrom, "NIST Chemistry WebBook, NIST Standard Reference Database 69," (1997).

[128]G. P. Dubey and M. Sharma, "Excess Volumes, Densities, Speeds of Sound, and Viscosities for the Binary Systems of 1-Octanol with Hexadecane and Squalane at (298.15, 303.15 and 308.15) K," International Journal of Thermophysics **29**, 1361–1375 (2008).

[129]D. Ducoulombier, H. Zhou, C. Boned, J. Peyrelasse, H. Saint-Guirons, and P. Xans, "Pressure (1-1000 bars) and temperature (20-100.degree.C) dependence of the viscosity of liquid hydrocarbons," The Journal of Physical Chemistry **90**, 1692–1700 (1986).